International Journal of Coal Geology 167 (2016) 184–200

Contents lists available at ScienceDirect

International Journal of Coal Geology

journal homepage: www.elsevier.com/locate/ijcoalgeo

Secretory organs: Implications for lipoid taxonomy and kerogen formation (seed ferns, Pennsylvanian, Canada)

Erwin L. Zodrow [a], José A. D'Angelo [a,b,*], Wilson A. Taylor [c], Tiziano Catelani [d,e], José A. Heredia-Guerrero [f], Maria Mastalerz [g]

[a] Palaeobiology Laboratory Cape Breton University, Sydney, Nova Scotia, Canada
[b] IANIGLA-CCT-CONICET-Mendoza-Área de Química, FCEN, Universidad Nacional de Cuyo, M55002JMA Mendoza, Argentina
[c] Department of Biology, University of Wisconsin-Eau Claire, Eau Claire, WI 54702-4004, USA
[d] Electron Microscopy Laboratory, Nanochemistry, Istituto Italiano di Tecnologia, Genoa, Italy
[e] Department of Earth Sciences, Università degli Studi di Firenze, Florence, Italy
[f] Smart Materials, Istituto di Tecnologia, Genoa 16163, Italy
[g] Indiana Geological Survey, Indiana University, 611 North Walnut Grove, Bloomington, IN 47405-2208, USA

ARTICLE INFO

Article history:
Received 12 July 2016
Received in revised form 27 September 2016
Accepted 12 October 2016
Available online 13 October 2016

Keywords:
Eigenchemistry
Secretory organs
Microstructure
Chemistry
Taxonomy
Kerogens

ABSTRACT

Secretory organs likely evolved with land plants in Silurian-Devonian time, but it is questionable if they were passed on to living cycadaleans upon the extinction of seed ferns (Triassic-Jurassic?). They are defined as ducts of schizo-, lysig- or rhexigenous origin that exuded a heterogeneous lipoid mixture that fossilized as secretory products (droplets). In this study we detailed (1) the physical properties and distributions based on the compression-preserved *Neuropteris ovata* var. *simonii* and *Laveineopteris rarinervis* frond sections (Late Pennsylvanian Sydney Coalfield, Canada). Examined were also 1300 cuticular slides representing a number of plant groups, complemented by published data to infer biomass accumulation as potential kerogen in the geological column. In addition, (2) from select pinnules of the two species mentioned, nine secretory products and four surrounding cuticles were analyzed by micro-FTIR to evaluate statistically (PCA) the chemotaxonomic potential, and the kerogen chemistry. Further studies in support of (1) or (2) included methods of NICI, SEM, TEM and AFM, and by EDS.

Results indicate that the secretory organs occurred in the entire *N. ovata* frond, its associate petiole and trunk, and in great abundance on the pinnules of both species in a random fashion. Secretory products show layering effects, surfaces can be intact, convoluted, folded, or damaged. At 100,000 magnification, microstructures are not observable. The exact chemical composition is unknown because of insolubility. IR spectra show peaks of functional groups frequently found in isocyanates, disubstituted alkynes, nitriles, polyynes, thiocyanates, and allenes, in part underpinned by EDS results. These compounds were presumably derived from the diagenetic alteration of resin-like terpenoid- or phenolic-related structures. That is particularly the case for the polyynes (i.e. 'polyacetylenes'), synthesized by living plants with a variety of biological functions, including pigments and flavorings, toxins, and chemical repellents.

The chemical information of the lipoid exudate, together with their morphological information and distribution will contribute to (i) the progress of chemotaxonomy and systematics of plant fossils, and (ii) a better understanding of the genesis of kerogens from plant-derived materials, particularly resinous remains.

1. Introduction

The study history of the black 'dots', 'punctuations' or 'Punktierung' on cuticles originated with certain Carboniferous seed ferns. Its history can be divided into two periods: 1867–1928 and 1929–2015. These coincide with progressive understanding of their nature due to advancing technical inventions, particularly in compound-light, scanning and transmission electron microscopies, Nomarski interference-contrast illumination (since 1955), and in infrared spectrometry.

For the period up to 1928, Bode (1929) summarized the interpretations of the black 'dots' as being, for example, sporangial seats, sori, hairy bases, *Spirorbis* sp., 'Eisenoxyde' (iron oxide), or fungal remains (Wang, 1997: fungal remains of Pl. 5, 2, 1997, and Kögel-Knabner et al., 1994, Fig. 2(d) are suspect of being secretory organs). In that seminal paper, Bode claimed that 'Drüsen' are not sporadic in [sic extant] plants '…

* Corresponding author.
E-mail addresses: zzodrovii@gmail.com (E.L. Zodrow), joseadangelo@yahoo.com (J.A. D'Angelo), taylorwa@uwec.edu (W.A. Taylor), Tiziano.Catelani@iit.it (T. Catelani), jose.guerrero@iit.it (J.A. Heredia-Guerrero), mmastale@indiana.edu (M. Mastalerz).

http://dx.doi.org/10.1016/j.coal.2016.10.004
0166-5162/

sondern für ganz bestimmte Pflanzenarten charakteristisch ist.' He also established basic parameters upon which the present paper is built. These include their organic (chemical) nature by observing that after applying Schulze's process to coalified (compression) specimens of the seed fern *Mariopteris latifolia* Brongniart, the black 'dots' [and the cuticle] had survived this brutal oxidative treatment. From the experiments he hypothesized that (1) a fundamental chemical difference existed between the coal-compression matter and the 'dots', (2) 'dots' compare with 'Drüsen' (secretory organs) of the angiospermous species *Hypericum perforatum* or St. John's Wort (Bode, 1929, Fig. 1), and that (3) their chemical makeup comprises bitumen, oils, resins, or waxes; for short ethereal oils. In hindsight, he had described a secondary metabolite in fossilized form for the first-time.

For the period 1929–2015, 'dots' were of little interest to palaeobotanists, except observations by Leisman (1960) regarding the cells of the upper epidermis of *Callipteridium sullivanti*, that were usually filled with a dark substance similar to that found in the secretory canals, hence probably representing a 'gummy or resinous deposit', and by Barthel (1961, 1962). Litke (1966, p. 352, Pl. XIV, 1; XV) recognized the occurrence of 'extranuptialen Nektarien' in liana-type fossils in brown coal of Miocene age (20–5 Ma). Šimůnek (1996, Plate 1, Fig. 7) correctly identified 'exit pores', and Pryor (1990, Fig. 13) documented 'dot' preservation of *Neuropteris* Brongniart in coal balls. Krings (2000), on the other hand, discussed secretory cavities, accompanied by light photography, from the perspective of secondary metabolites, analogous with functions in extant flora. He argued against [palaeo] taxonomic utility, in the absence of analytical data from fossil flora.

This paper initiates a new period in the study of 'dots' for which we use the name secretory organs. In particular, those from the foliage of the two larger frond segments of the seed-ferns *Neuropteris ovata* (Hoffmann, 1827) var. *simonii* (Bertrand, 1930) Zodrow *et* Cleal 1998, and *Laveineopteris rarinervis* (Bunbury, 1847) Cleal et al., 1990, hereafter referred to as *N. ovata* and *L. rarinervis*, respectively, were investigated in detail. The analytical techniques include Nomarski interference-contrast illumination (NICI), scanning electron microscopy (SEM), transmission electron microscopy (TEM), atomic force microscopy (AFM), X-ray energy dispersive spectroscopy (EDS), and Fourier transform infrared spectroscopy (micro-FTIR).

Our contributions consist of (i) describing the physical nature and distribution of secretory organs in the two study species, assessing Carboniferous-Triassic occurrence/distribution based on cuticular analysis of 1300 thin sections housed at Cape Breton University, (ii) hypothesizing secretory organs as kerogen contributor to oil generation in sedimentary rocks (see D'Angelo et al., 2010), and (iii) showing their potential for lipoid chemotaxonomy based on chemometric arguments. We caution, however, that "… a relationship between source rock and rock kerogen cannot be directly established in most cases." (*in litt*., Dr. C. Eble, 2016).

At the same time, this study highlighted challenges of working with heretofore undetermined and poorly-documented fossilized organic material, although we considered models which included resins and essential oils (e.g., Lyons et al., 1982; Chadwick and Whelan, 1992; van Bergen et al., 1995; Tsubaki and Azuma, 2013; Adinew, 2014).

2. The data base, and sample preparation

2.1. The extensive data base for secretory organs

The senior author collected large numbers of Carboniferous compression-plant fossils from the Sydney Sub-Basin of the Maritime Carboniferous Basin (Figs. 1 and 2). This includes the largest known *N. ovata* frond segment of 65 cm, with cyclopteroid pinnules organically attached to an associate petiole and trunk from the Point Aconi Seam (Zodrow and Cleal, 1988, Pls. 2–4), and the 45-cm long bipinnate *L. rarinervis* specimen from the Lloyd Cove Seam (Fig. 3A and B, respectively). Included in the collection are compression specimens from the Mabou Sub-Basin (Zodrow and Vasey, 1986), the Stellarton Sub-Basin (Lyons et al., 1997; Zodrow et al., 2000), and the Bay St. George Sub-Basin (Zodrow et al., 2000; Bashforth, 2005), see Fig. 1. Specimens of Indiana 'paper' coal (DiMichele et al., 1984), *Dicroidium* flora of Argentina (D'Angelo et al., 2011), and extant foliar and ovular specimens of *Cycas rumphii* Miquel, and ovular specimens of cycadealean *Zamia furfuracea* L. filius, and *Encephalartos ferox* (Bertol) are also part of the collection.

From these specimens, the senior author had prepared ca. 1260 representative cuticular glass-mounted slides. With the addition of 40 cordaitean slides (Šimůnek, 1996), the data base comprised 1300 slides, curated at Cape Breton University. By far the largest number of slides contain cuticles from pinnules and other organs of seed ferns, followed by cordaiteans, and distantly by ferns and lycopsid. Other organs (160 slides) refer to the constituents of macerated trigonocarpalean ovules and cuticles associated with, but not attached to medullosalean fronds (Cleal et al., 2010; Zodrow et al., 2013, 2014) that were used to further test the distribution of secretory organs in the [female] reproductive organ of seed ferns. From living cycadealean foliar and ovular materials (80 slides) were also included to test for the presence of secretory organs in the presumptive closest living relative to the extinct medullosaleans (cf. Zodrow and D'Angelo, 2014, p. 839). Routinely examined for secretory organs were ovules of *Zamia furfuracea* L. filius and *Encephalartos ferox* (Bertol). Results are tabulated in Supplementary material, Table 1.

2.2. Preservation and sample preparation

The *N. ovata* and *L. rarinervis* specimens were deposited in a fine-grained sandstone of basal Cantabrian age in a slowly subsiding coastal plain (Forgeron et al., 1986), forming the non-marine Sydney Sub-Basin (see Calder, 1998). A vitrinite-reflectance value of Ro% 0.75 points to conditions for favorable compression/coalification preservation for the secretory organs (cf. Hacquebard, 1984, Fig. 3).

Secretory organs specifically for the analytical experiments were obtained from macerating select *N. ovata* pinnules for 25–45 min, and *L. rarinervis* pinnules for seven hours. Sample locations are marked in Fig.3A and B, respectively. Since the secretory organs occurred internally (e.g., Fig. 4), separating cuticles into lower and upper surfaces was necessary to expose them for analyses by micro-FTIR, EDS, SEM, and AFM. For TEM, however, cuticles remained intact to be able to ascertain upper and lower cuticle/secretory organ boundaries in situ.

3. Analytical methods

Imaging and measurements of secretory organs were carried out at 250 or 500 magnification using a biological microscope equipped with a digitizing camera and NICI.

Micro-FTIR is a tool especially designed for obtaining chemical information from small objects, and the 10–117 μm diameter secretory organs fit well micro-FTIR capabilities (cf. Mastalerz and Bustin, 1993a; Smith, 1996, p. 157; Heredia-Guerrero et al., 2014; Chen et al., 2015). A Nicolet 6700 spectrometer connected to a Nicolet Continuum microscope operated in reflectance mode was used to generate the data. The microscope was connected to a liquid, nitrogen-cooled mercury-cadmium-telluride (MCT) detector. Micro-FTIR spectra were obtained at a resolution of 4 cm^{-1} over the range 4000 cm^{-1} to 600 cm^{-1} wavenumber, using a gold plate as background. An OMNIC program was used for spectral processing.

The interpretive aspect of the IR spectra entailed two complementary, commonly used approaches in our FTIR work: (1) qualitative and (2) quantitative. (1) Involved routine IR-peak assignments of functional groups (structural parts of molecules or moieties), as well as groups and classes of compounds (Table 1), following published sources, for example Wang and Griffiths (1985); Colthup et al. (1990); and Rochdi and Landais (1991). (2) Involved mathematical treatment applied to the digitized spectra to calculate 11 semi-quantitative IR ratios. The

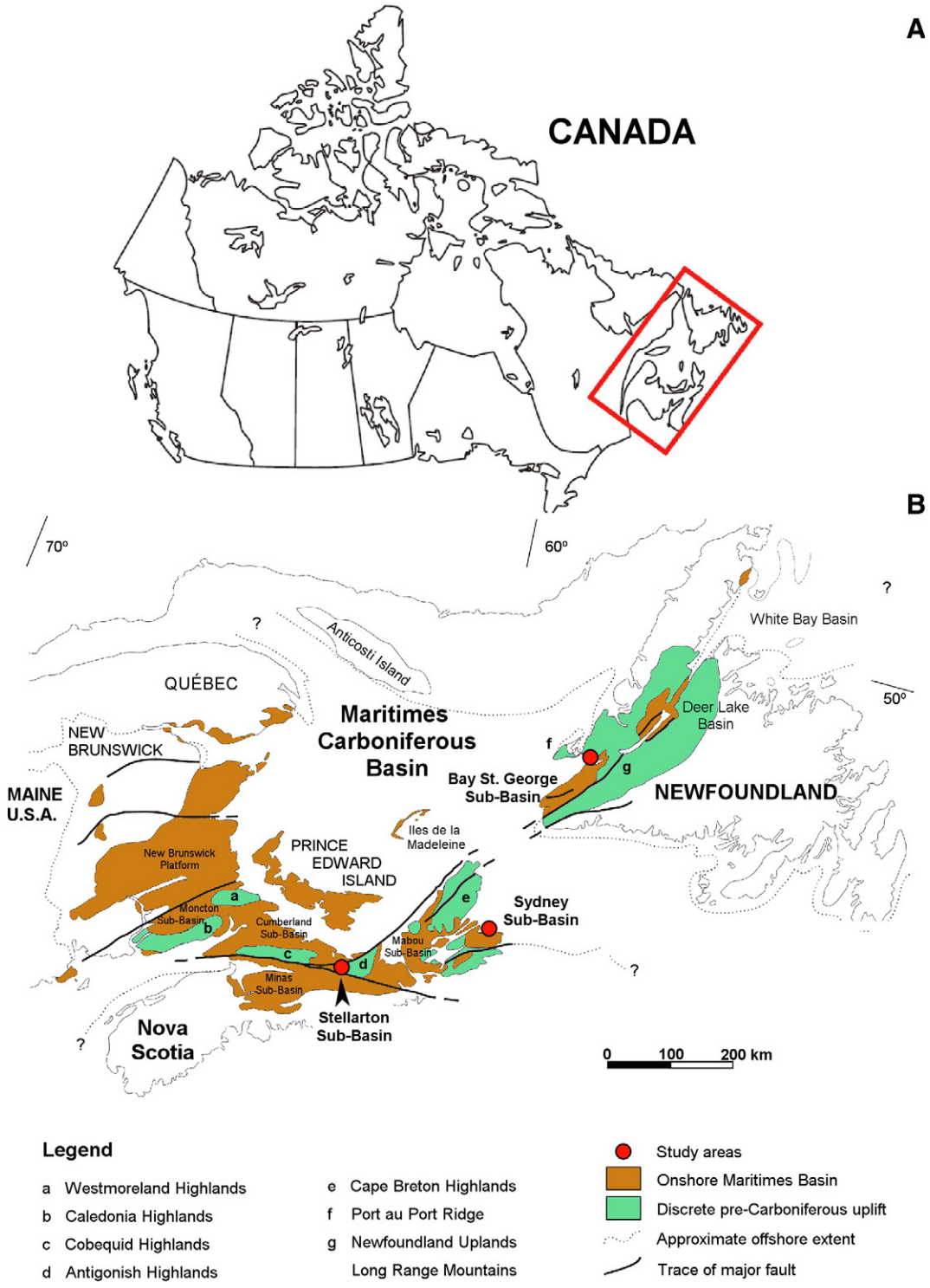

Fig. 1. Location map. (A) Canada. (B) Maritimes Carboniferous Basin (Roliff, 1962), and sampled three Sub-Basins (marked red disks).

methylene/methyl CH_2/CH_3 ratio was calculated after Fourier self-deconvolution (Kauppinen et al., 1981a, 1981b) of the aliphatic C=H stretching region (3000–2800 cm-1) into individual peaks (see Lin and Ritz, 1993a, 1993b; Zodrow and Mastalerz, 2007). Other semi-quantitative parameters included C=O, aromatic carbon (C=C), and the combined contribution of C=O, C=C, and other oxygen-bearing compounds (Ox: Table 2) (cf. Sobkowiak and Painter, 1992; Mastalerz and Bustin, 1993a; and D'Angelo, 2006). Additional details and references about FTIR-derived parameters can be found in Ganz and Kalkreuth (1987); Colthup et al. (1990); Petersen et al. (2008); Petersen and Nytoft (2006).

Caution is advised when making comparisons of semi-quantitative, IR-derived data obtained with different FTIR techniques, e.g., KBr-pellet FTIR vs. reflectance micro-FTIR (present method) (see Mastalerz and Bustin, 1993b). Therefore, the presently-generated data may not be directly comparable with our previously published semi-quantitative data by the KBr-pellet method for fossilized cuticles (Zodrow and Mastalerz, 2009), compressions-cuticles, and coals. The micro-FTIR data were

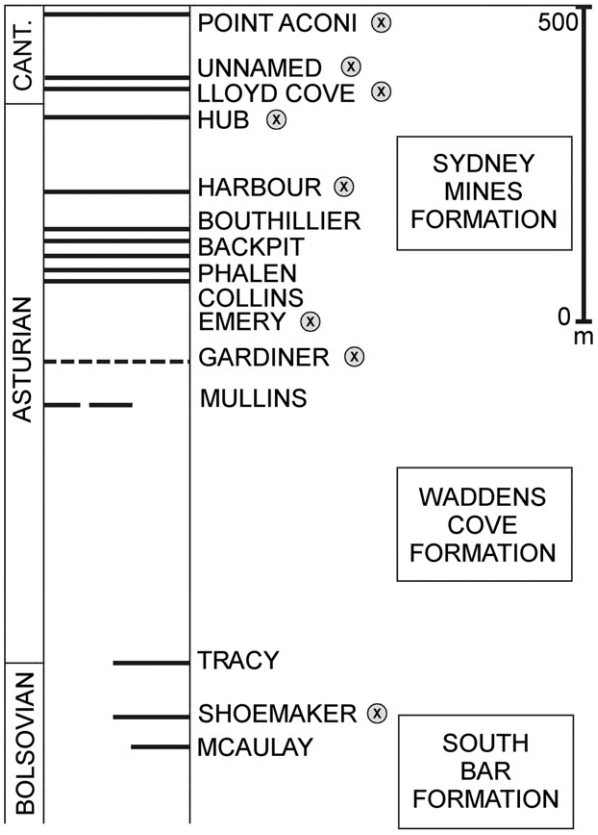

Fig. 2. Coal stratigraphy of 1200 m thick Sydney Sub-Basin, and occurrences of secretory organs (marked 'X'). Cant = Cantabrian.

statistically grouped using principal component analysis (PCA), noting that PCA matrices are omitted.

Though preliminary because of a smaller micro-FTIR sample (Table 2), the PCA results are nevertheless useful to place the data in the geochemical context for exploring potential chemotaxonomy (summary: D'Angelo et al., 2010).

EDS is an X-ray technique that allows the identification of particular elements, and by an areal scan produces a map of the relative intensity and distribution of elements. EDS analysis of a secretory organ was performed on a Pulse Tor ON-X system. Gold coating, 20 nm thick, was a necessary procedure, as non-coated secretory organs were virtually impossible to differentiate from the back ground of the cuticle.

For SEM analysis, high-resolution imaging was carried out using a Joel JSM 7500FA, equipped with a cold-field emission gun (FEG) which was operated at 15 kV accelerating voltage. The samples were coated with a 10-nm thick film of carbon using an Emitech K950X high vacuum turbo system. Imaging was performed in a secondary electron mode to analyze the detailed morphology of the samples. Some SEM images were also collected with a Pemtron PS-230 SEM using 20 kV accelerating voltage, and 60-nm thick gold coating.

AFM is designed to measure local properties such as height on a nanometer scale (this study). Such measurements were performed using an XE-100PSIA instrument, and the images were acquired in non-contact mode, working in air in a vibration-insulated environment (Table Stable TS-150). Single-beam silicon cantilevers coated with aluminum on the reflective side (type PPP-NCHR-10, Nanosensors) with a typical elastic constant of 42 N m^{-1} and a nominal tip radius of < 10 nm were used with a drive frequency of ~295 kHz. Measurements were taken at a scan rate of 0.2 Hz and 40 × 40 μm^2 of zoom.

For TEM analysis, secretory organs were stored in ethanol, and selected specimens were embedded in 4% agar to facilitate handling through subsequent solution changes. Acetone was used as a transitional solvent between 100% ethanol and unpolymerized epoxy monomer

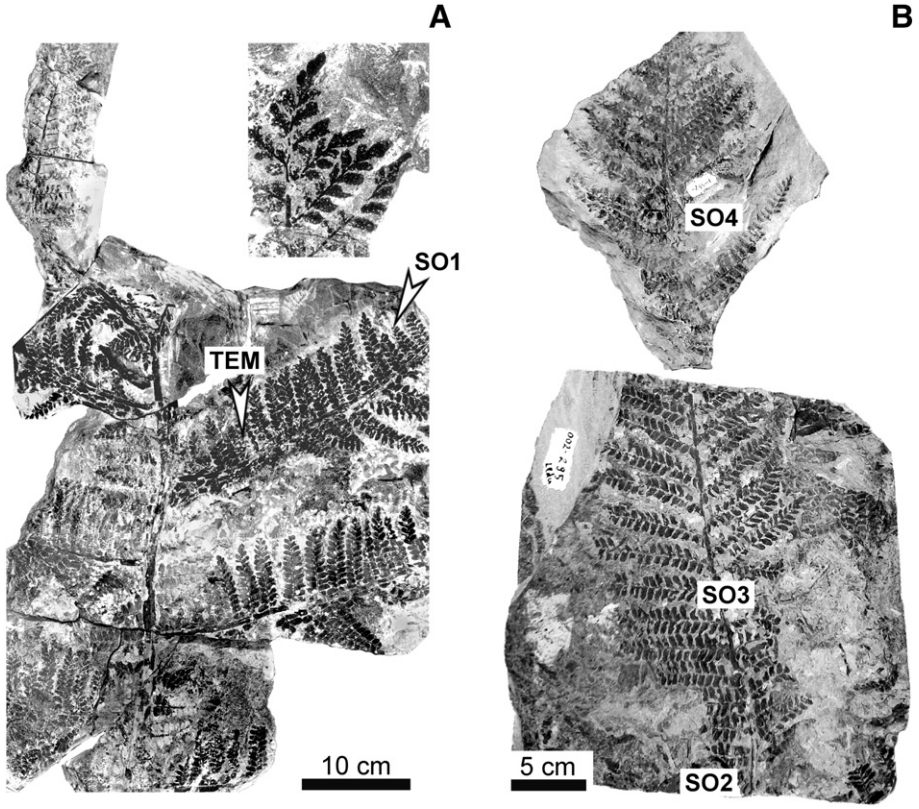

Fig. 3. Study specimens. (A) Frond of *N. ovata*. Samples: 'SO1' micro-FTIR; 'TEM' includes AFM microanalysis. (B) Penultimate pinna of *L. rarinervis*. Samples: 'SO2' micro-FTIR, TEM, and AFM microanalyses; also 'SO2' to 'SO4' for SEM imaging of secretory products. (A) Point Aconi Seam. (B) Lloyd Cove Seam.

Table 1
IR-peak assignments: *N. ovata* and *L. rarinervis*. Micro-FTIR spectra are divided into seven spectral zones (color-keyed to Figs. 11 and 12) in accordance with functional groups and classes of compounds.

Range/wavenumber (cm^{-1})	Group and class of compound	Assignment and remarks	Representative spectrum (example)	Spectral zone
2990–2850	$-CH_3$ and $-CH_2-$ in aliphatic compounds	CH antisymmetric and symmetric stretching	Fig. 11B, C, E	1
2850–2700	$-CH_3$ attached to O or N	CH stretching modes	Fig. 12F, G, H	1
2600–2500	–SH in alkyl mercaptans	S–H stretching	Fig. 11A, B, C, D	2
2285–2250	–N=C=O in isocyanates	N=C=O antisymmetric stretching	Fig. 12A	2
2260–2200	–C≡C in disubstituted alkynes, –C≡N in nitriles	C≡C stretching, C≡N stretching	Fig. 11A, B, C, D,	3
2200–2100	–C–C≡C in polyynes, –C≡N in thiocyanates	C≡C stretching, C≡N stretching	Fig. 12B, C	3
2000–1900	C=C=C in allenes	C=C=C antisymmetric stretching	Fig. 12D, E	3
1870–1650	C=O in carbonyl compounds	C=O stretching	Figs. 11 & 12 (A, B, C, D)	4
1772–1729	C=O in aliphatic esters	C=O stretching	Figs. 11 & 12 (A, B, C, D)	4
1719–1700	C=O in ketones + ?carboxylic acids	C=O stretching	Figs. 11 & 12 (A, B, C, D)	4
1690–1664	Conjugated C=O, quinone C=O	C=O stretching	Figs. 11 & 12 (A, B, C, D)	4
1654–1630	C=O in highly conjugated ketonic structures, H-O in phenolics	C=O stretching, H-O stretching	Figs. 11 & 12 (A, B, C, D)	4
1596–1585	Carboxyl + benzene ring in aromatic compounds	C=O stretching, C=C aromatic ring stretching	Figs. 11 & 12 (A, B, C, D)	4
1545–1500	Benzene ring in aromatic compounds	C=C aromatic ring stretching	Figs. 11 & 12 (A, B, C, D)	4
1460–1400	CH_3-, CH_2- in aliphatic compounds	CH_3-, CH_2- antisymmetric deformation	Fig. 11A, C, E	5
1377–1375	CH_3 in aromatic and aliphatic compounds	CH_3–Ar, R symmetric deformation	Fig. 12F, G, H	5
1279–1260	C–O in aromatic ethers	C–O stretching	Fig. 12H	6
1238–1218	C–O in phenoxy structures, C–O–C in aromatic ethers	C–O stretching, OH stretching, C–O–C antisymmetric stretching	Fig. 11E	6
1225–1200	C–O–C in vinyl ethers	C–O–C antisymmetric stretching	Fig. 12D	6
1168–1150	C–O in phenols, C–O–C in aliphatic ethers	C–O stretching, C–O–C antisymmetric stretching	Fig. 12D	6
1150–1030	C–O–C in aliphatic ethers, Si–O in silicates[a]	C–O–C antisymmetric stretching, Si–O stretching	Fig. 12A, E	6
1000–950	$CH=CH_2$ in vinyl compounds, CH=CH– in trans disubstituted alkenes	C=H out-of-plane deformation	Fig. 11D, E; Fig. 12D	7
850–790	CH=C in trisubstituted alkenes	C=H out-of-plane deformation	Fig. 11B; Fig. 12D, E	7
740–720	$-(CH_2)_n-$ in hydrocarbons	CH_2 rocking in methylene chains	Fig. 11E; Fig. 12E	7
870, 820, 755	$-(CH_2)-$ in aromatic hydrocarbons	C–H out-of-plane deformation	Fig. 11B; Fig. 12B, C	7

[a] Silicate impurities.

(modified Spurr; Ellis, 2006). Specimens were then placed over night at 60 °C into pure resin in aluminum-weighing dishes with the proper orientation for sectioning and polymerization. Proper orientation entailed sectioning parallel to the cuticle and across it. Gold and silver sections were cut using a Leica Ultractut UCT, and sections collected on 2 × 3 mm slot grids coated with formvar. Sections were subsequently viewed in a Joel 2010 TEM operating at 80 kV, and images captured using a side-mounted digital camera (AMT, Woburn, MA, U.S.A.).

Fig. 4. Occurrence of a secretory product (arrowed) on one internal rachial cuticle of an intact ultimate pinna of *Macroneuropteris macrophylla* (Brongniart). 'M' marks the rachial margin. Temporary slide 009-200 (Lloyd Cove Seam). Photographed under water.

4. Results

Since a number of analytical approaches were used with bearing on unraveling the nature of secretory organs in situ, contributory results are separately described. Summarized in Section 4.1 are the physical attributes, distributions (NICI), and pit falls of identification of secretory organs; in Section 4.2 their structure by methods of SEM, AFM and TEM from *N. ovata* and *L. rarinervis*; in Section 4.3 the chemical results from the lipoid perspective (see Fahn, 1979); and in Section 4.4 elementary distribution over a surface of a secretory organ.

4.1. Bio-physicochemical characteristics and general sample statistics

The examination of hundreds of secretory organs in the secretory-organ data base by NICI resulted in identifying a number of characteristics. One of them is that a fossilized secretory organ consists of a secretory duct that exuded secretory products. The latter are typically opaque, vitreous, dark amber in color occasionally, and invariably spheroidal (see SEM). They are chemically indestructible by the grueling oxidative-alkaline treatment (Schulze's process), even after a week's treatment, thus resembling the chemical inertness of sporopollenin (Barrier, 2008). However, fractured dried secretory products resembled the fractural characteristics of vitrain.

Loose secretory products may be difficult to distinguish from small coaly particles even at 45 magnification. They are not visible on compressions, even when HF-liberated from the rock matrix, but are on naturally macerated cuticles (Fig. 5A). Secretory products of differing sizes, representative of different species and their organs from Laurasia and Gondwana, are illustrated in Fig. 5B to L. Peripheral laceration of the pinnule cuticle about secretory products is frequently observed (e.g., Fig. 5B), whereas it does not occur on the thicker rachial cuticles (e.g., Fig. 5C).

Table 2
Micro-FTIR: Semi-quantitative chemistry for secretory products of *N. ovata*: NoSP1 NoSP4, where *NoCut* is the cuticle next to an unspecified NoSP, and of *L. rarinervis*: LrSP1 LrSP5, where *LrCut1* to *LrCut3* are the cuticles next to three unspecified LrSP's. Sydney Coalfield, Canada.

Secretory product and cuticle Sample number	CH_2/CH_3	CH_{al}/Ox	C=O/C=C	C=O cont	C=C cont	CH_{al}/C=C	'A' factor	'C' factor	CH_{al}/C=O	CH_{ar}/CH_{al}	CH_{ar}/C=C
N. ovata											
NoSP1	1.5	0.15	1.4	0.2	0.12	1.22	0.55	0.59	0.9	2.00	2.45
NoSP2	0.7	0.17	7.4	0.3	0.04	4.81	0.83	0.88	0.7	0.34	1.65
NoSP3	3.1	0.45	2.5	0.1	0.06	7.94	0.89	0.72	3.1	0.36	2.85
NoSP4	1.0	0.05	1.7	0.2	0.10	0.54	0.35	0.63	0.3	4.96	2.66
NoCut	0.5	0.13	4.7	0.2	0.05	2.62	0.72	0.82	0.6	1.13	2.96
L. rarinervis											
LrSP1	2.0	0.14	10.0	0.2	0.02	5.99	0.86	0.91	0.6	1.75	10.48
LrSP2	2.9	0.14	6.0	0.2	0.03	3.95	0.80	0.86	0.7	1.04	4.11
LrSP4	0.7	0.12	VH[a]	0.3	0.01	8.30	0.89	0.95	0.4	0.12	1.01
LrSP5	2.4	0.10	VH[a]	0.2	0.02	6.58	0.87	0.92	0.6	0.07	0.45
LrCut1	5.6	0.58	2.0	0.1	0.06	9.29	0.90	0.64	5.2	0.35	3.23
LrCut2	5.6	0.39	0.8	0.06	0.07	5.52	0.85	0.45	6.8	0.03	0.15
LrCut3	5.9	0.39	0.8	0.05	0.06	6.28	0.86	0.44	8.1	0.01	0.08

LrSP3 is not included in the semi-quantitative analysis because of the poor qualitative spectrum (i.e., peak-area calculations are unreliable), but its spectrum is shown (Fig. 12C).
[a] VH = very high values (i.e., higher than 1000).

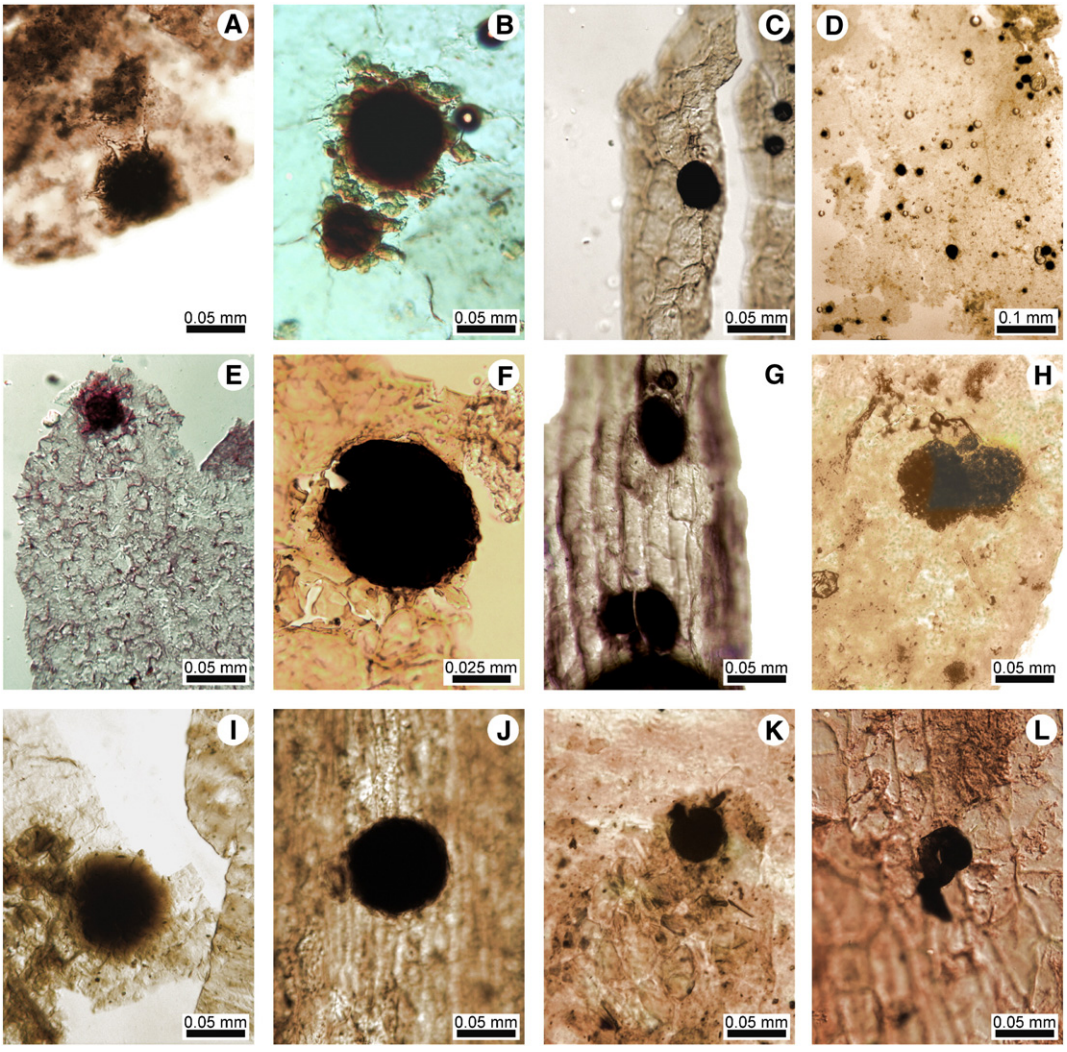

Fig. 5. Illustrating size variation and occurrence of secretory products on diverse plant-fossil organs from Canada (Ca), the Czech Republic (Cz), Indiana 'paper' coal (USA), and Argentina (Ar). (A) *Odontopteris cantabrica* (Wagner), fossilized pinnule cuticle (Ca). (B) *L. rarinervis*, pinnule (Ca. Fig. 3B, marked 'SO4'). (C) *M. macrophylla*, cyclopteroid pinnule below the main frond dichotomy (Ca). (D) *L. rarinervis*, see (B). (E) *N. ovata*, adaxial pinnule (Ca) (Fig. 3A, lower frond part). (F) *M. macrophylla*, see (C). View of a secretory product opposite to entry into the cuticle (Ca). (G) *Alethopteris ambigua* p. (Lesquereux), ultimate pinna rachis (Ca). (H) *Lonchopteridium karvinesis* (Purkyňová), pinnule (Ca). (I) *Cordaites principalis* (Germar), leave (Cz). (J) *C. principalis*, leave (Ca). (K) *Karinopteris* Boersma sp., pinnule (USA). (L) *Dicroidium* Gothan sp., pinnule (Ar). Slides (A): 81-458 xxx NMC; (B) 02-295-1 rari; (C) 3-337/5a macro; (D) 002-295-1 rari; (E) 85-248/6; (F) 3-337/4 X M. macro; (G) Marked '0' 84-520/2; (H) 989-303/11; (I) Slide 2 Czech. (J) BB-30-228/1 (1); (K) Indi/5; and (L) NMC-3/2, respectively.

Generally, secretory products occurred internally on abaxial pinnule cuticles, occasionally on an inner adaxial surface as is shown in Fig. 5E for *N. ovata* with its typical sinusoidal anticlinal walls, or internally on both cuticular surfaces of ultimate, penultimate and antepenultimate rachides. Midveins are consistently secretory organ-free, as are lateral veins. An underside of a secretory product is shown in Fig. 5F, where the periphery is noticeably intact. In unseparated cuticles secretory products appeared diffused without a sharp periphery (e.g., Fig. 5I). The *Dicroidium* flora of Argentina is represented in Fig. 5L (D'Angelo et al., 2011). We concur with Bode's (1929) observation that secretory organs did not occur on external cuticular surfaces.

Diameters of the secretory products from the different architectural parts of the *N. ovata* frond differ little from one another, and from the diametric average of ca. 56–60 μm in *L. rarinervis*, except that for the latter species sample variability is probably larger (cf. Fig. 5B; Supplementary material, Table 1). A sample from a foliar cuticle of *L. rarinervis* in Fig. 5D underscores densely distributed secretory products of variable diameters.

4.1.1. Secretory ducts

The distinction between secretory ducts and secretory products corresponds with the tenets of modern plant-cell anatomy, identifying three passageways (Braune et al., 1999, p. 77). These are (1) schizogenous (cellular separation by dissolution of interlaminae), (2) lysigenous (dissolution of intercellular walls), and (3) rhexigenous (broken and lacerated cellular material). Each one of them is assumed suitable for serving as an effective fossil secretory duct; see Fahn (1979) for detailed discussion concerning extant flora. What we have found fossilized and interpreted accordingly as ducts is summarily illustrated in Fig. 6, based on NICI. The physical removal of a secretory product from an ultimate-pinna rachis exposed a closed duct (30 μm in diameter) with what appeared to be a sutural line 'X' surrounded in part by a 'dentate collar' (Fig. 6A). A similar situation is illustrated in Fig. 6B on an abaxial pinnule of *Macroneuropteris scheuchzeri* (Hoffmann) where the duct shows in situ micron-sized fossilized droplets: compare with Fig. 6G–I. A 'dentate collar' is also present on an abaxial pinnule of *Dicroidium* (Gothan) sp. from the Argentine Triassic rocks (Fig. 6C). About 40 μm distant from the 'dentate collar' occurred a 24-μm diameter duct that is shown in Fig. 5L.

A ca. 60-μm diameter secretory product emerging from a ca. 30-μm diameter duct is documented on an abaxial, intercalary pinnule of *N. ovata* (Fig. 6D). It is noted as an open, circular secretory duct, with a faintly outlined 'dentate collar'. A large secretory product (ca.74-μm diameter) in Fig. 6E shows what appear to be evenly-spaced perforations (<1 μm in diameter) in the surrounding cellular tissue (cf. SEM Fig. 8C and F).

In contrast with the 'dentate-collar' configuration, some ducts showed relatively smooth cuticle-exit edges exemplified by the 23-μm diameter duct in *M. scheuchzeri* (Fig. 6F). However, others on the same slide show 'dentate collars'. Developing secretory products that were

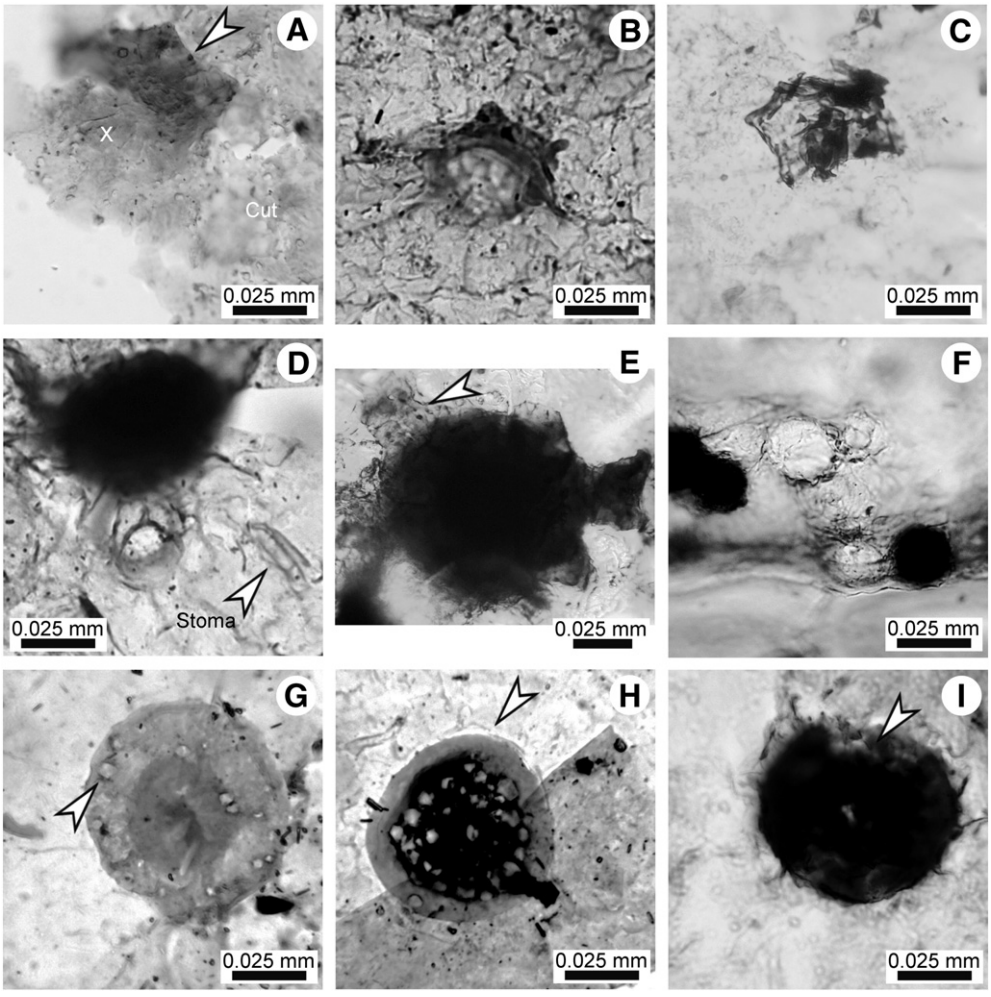

Fig. 6. Illustrating secretory ducts and developing secretory products there from, Canada (Ca) and Argentina (Ar). (A) *N. ovata*, ultimate rachis (Ca). A closed duct with a suture? (marked 'X'), ultimate rachis, 'dentate collar' (arrowed), and Cut = cuticle. (B) *M. scheuchzeri* (Hoffmann), pinnule (Ca). Emerging secretory product (droplets) in situ. (C) *Dicroidium* sp., pinnule (Ar). (D) *N. ovata*, intercalary pinnule (Ca). Emerged secretory product. A stoma is arrowed. (E) *N. ovata*, pinnule (Ca). Upper left (arrowed), perforated collar. (F) *M. scheuchzeri*, pinnule (Ca). (G) and (H) *L. rarinervis*, pinnules (Ca). Developing droplets, arrowed. (I) *N. ovata*, pinnule (Ca). Partially exposed droplets (arrowed). Slides: (A) Ur Pi 85-248/10c; (B) 977-427a/2; (C)NMC-3/2; (D) and (E) Pin 85-246/6 and 7; (F) 1/2Pinnule/4; (G) and (H) CCB982-275/4 and 5; and (I) 85-248/TI, respectively.

fossilized in situ at differing exuding stages are documented in Fig. 6G–I. Initial formation of micron-sized droplets is illustrated in Fig. 6G (arrowed) that progressively increased in density? and diameter (Fig. 6H). In Fig. 6I coalescence and 'capping' had occurred, leaving open a very narrowed duct in the center for possibly repeated flows to form a complete secretory product. Fig. 6G and H are from the same slide (*L. rarinervis*), and Fig. 6I is from *N. ovata*.

4.1.2. Distribution of secretory organs

Fig. 2 summarizes the stratigraphic distribution of secretory organs in the Sydney Sub-Basin, noting their presence in the long-ranging *Macroneuropteris scheuchzeri* taxon (cf. Supplementary material, Table 1).

In particular, these organs are distributed over the entire *N. ovata* frond, including the associate petiole with attached cyclopteroids, and the trunk, and over the bipinnate *L. rarinervis* specimen. They occur in masses in the pinnules, less so on the rachides. The rare occurrence of secretory organs on the integument of *Trigonocarpus* sp. (not illustrated; slides 85-202/3 and 85-2002/4: cf. Zodrow et al., 2013), though significant in itself in the understanding of their distribution in a mother-plant fossil, requires confirmation. On the other hand, the sample foliage and ovules of *C. rumphii*, and ovules of *Z. furfuracea* and *E. ferox* provided no evidence for the presence of secretory organs.

Based on the overall observations in *N. ovata* and *L. rarinervis*, a trend is neither discernible in the pinnules nor in the rachides, suggesting a random distribution of secretory organs. Noted is that for the species in the slide-data base, other than *N. ovata* (Supplementary material, Table 1), either insufficient sample material is available to warrant statements about abundance, or occurrences are indeed rare as observed. Taking into account that the *N. ovata* specimen represents a much larger portion of the mother frond than the penultimate pinna of *L. rarinervis*, it is nevertheless instructive to note that the latter has a comparatively more erratic distribution, where on some pinnules secretory organs were absent, and on others abundant (e.g., Fig. 5D).

4.1.3. Pit-falls for identification

In certain instances, even when magnified ×125, structural holes of 20–30 μm diameter show 'dentate collars' in cuticles from different species (e.g., Fig. 7A and B). The question that arises is if such a configuration (e.g., Fig. 6A to D), is necessarily a structural part, or indicative of a duct, in the absence of a confirmatory secretory product? That this is not the case is illustrated by a 'dentate collar' about (1) a truncated trichome in situ on the pinnule of *M. macrophylla* (Fig. 7C), and (2) a sunken stoma on the abaxial surface of the cycadealean foliage that bears *C. rumphii* fructification (Fig. 7D). However, Degani-Schmidt and Guerra-Sommer (2016, Pl. 5, Fig. 1; Pl. 9, Fig. 4) observed 'filamentous projections' [our 'dentate collars'?], in the absence of what we call a secretory product, in association with 'secretory cavities'.

It is also commonly assumed that structural holes positioned along a pinnule margin, particularly in seed ferns, represent hydathodes (cf. Fahn, 1979; Cleal and Shute, 2012). But Fig. 6F

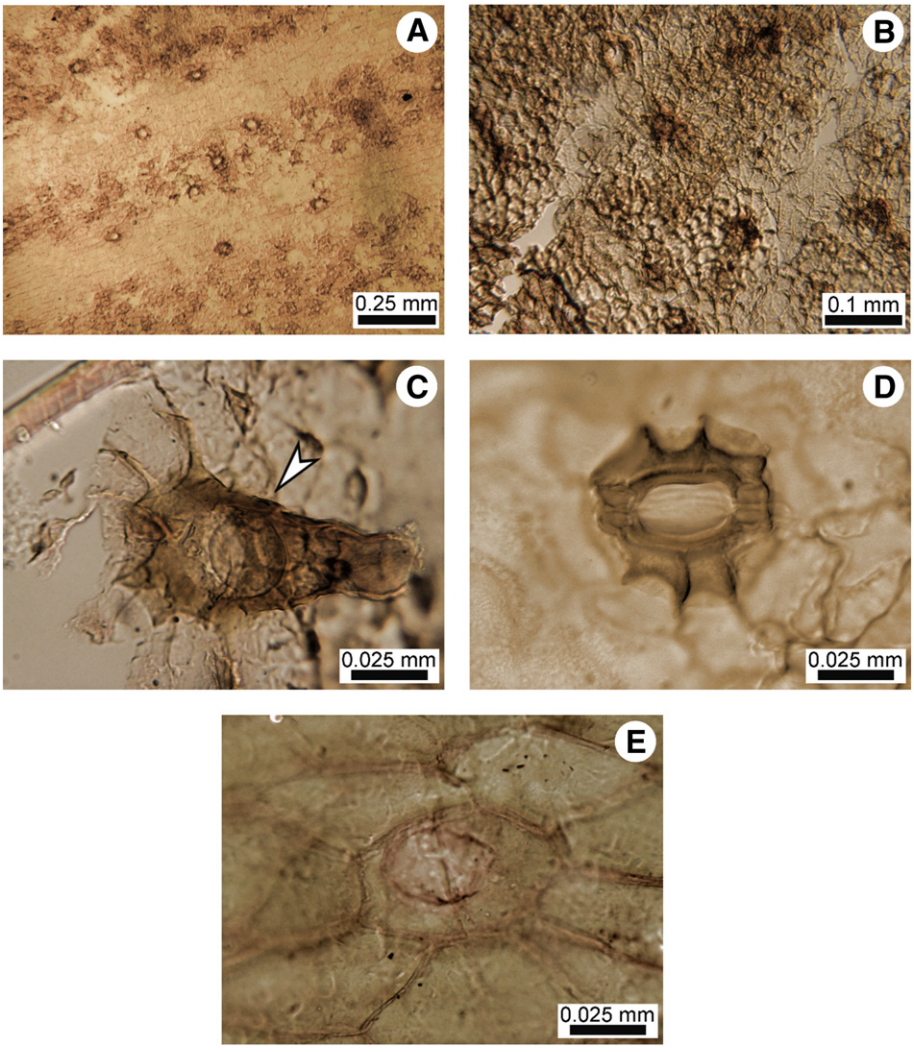

Fig. 7. Deceptive duct structures. *M. macrophylla*. (A) and (B) Pinnules above, and (C) below the main frond bifurcation (Ca). (D) *Cycas rumphii* foliage, stoma, lower cuticle. (E) *A. ambigua* p. penultimate rachis (Ca). Arrow points to a trichome. Slides: (A) 02-352/1; (B) 09-200/2; (C) 03-337a/2 TRICH X; (D) Crfoliage/13 LoCut; and PUr 4 84-520-0/10a, respectively.

demonstrated that secretory products and round 'non-dentate' ducts coexist separated by a few microns, inferring that position alone of such marginal structures cannot routinely be assumed to represent hydathodes, as secretory organs cannot categorically be ruled out. However, analogously to extant flora, both ducts and hydathodes are secretory organs that exude liquid substances, lipoids from the former and aqueous from the latter (cf. Fahn, 1979). Lastly shown in Fig. 7E is an example of a sunken, round feature (27 μm in diameter) with a suture? oriented across the elongate cellular pattern that could, amongst others, be interpreted as a stoma or a duct *sans* 'dentate collar'.

4.2. SEM

SEM images of secretory products are shown in Fig. 8 for the first time. Although they consistently appear spheroidal in NICI as noted, SEM shows variable spheroidal–oblate spheroidal–ellipsoidal–hemispheroidal bodies. The first six (Fig. 8A to F) are from *N. ovata* (i.e., location is marked 'SO1' on Fig. 3A). Instructive is Fig. 8A as it shows, though faintly, centrally located remnants of micron-sized droplets that on morphological grounds can be directly related to those shown in Fig. 6H. A distinctly preserved layering effect with sub-micron sized, round features is visible in Fig. 8B, whereas Fig. 8C depicts an intact secretory product with perforations occurring regularly about the periphery in the cuticle. Images (Fig. 8D to F) originated from rachides and the petiole of the *N. ovata* frond. A 42-μm diameter secretory product on a penultimate rachis is documented (Fig. 8D) that shows at 1700 magnification no evidence for a collapse structure, an intact topography, and evidence for a 'dentate collar' (see the EDS spectrum, Fig. 13). Equally intact on an antepenultimate rachis is a slightly oval-shaped, 42-μm diameter secretory product with evidence for layering (Fig. 8E). Noticed are the highly cutinized cellular walls, comparable to expressions in extant plants (cf. Braune et al., 1999, Abb. 67). A secretory product on the petiole (Fig. 8F), in contrast, has a folded and somewhat convoluted topography, but it best illustrates the regular arrangement of the peripheral perforations.

The remaining three images (Fig. 8G to I) show secretory products on pinnules of *L. rarinervis* (marked 'SO2 to SO4' on Fig. 3B). A small one with an ideal circular shape, but very much folded (indented?) topography, is evident (Fig. 8G). This also illustrates a rhexigenous origin attested to by the lacerated cuticle. Imaged in Fig. 8H is a large, badly damaged secretory product that at the same time revealed an internal relic-layered structure without evidence for folding. Fig. 8I shows two secretory products of differing diameters separated by ca. 100 μm (cf. Fig. 5D); particularly the larger right-hand one shows a layered structure.

4.2.1. AFM

The problem encountered by the 3D mapping of the secretory-product surfaces was the relief (local high-low elevation differential) that

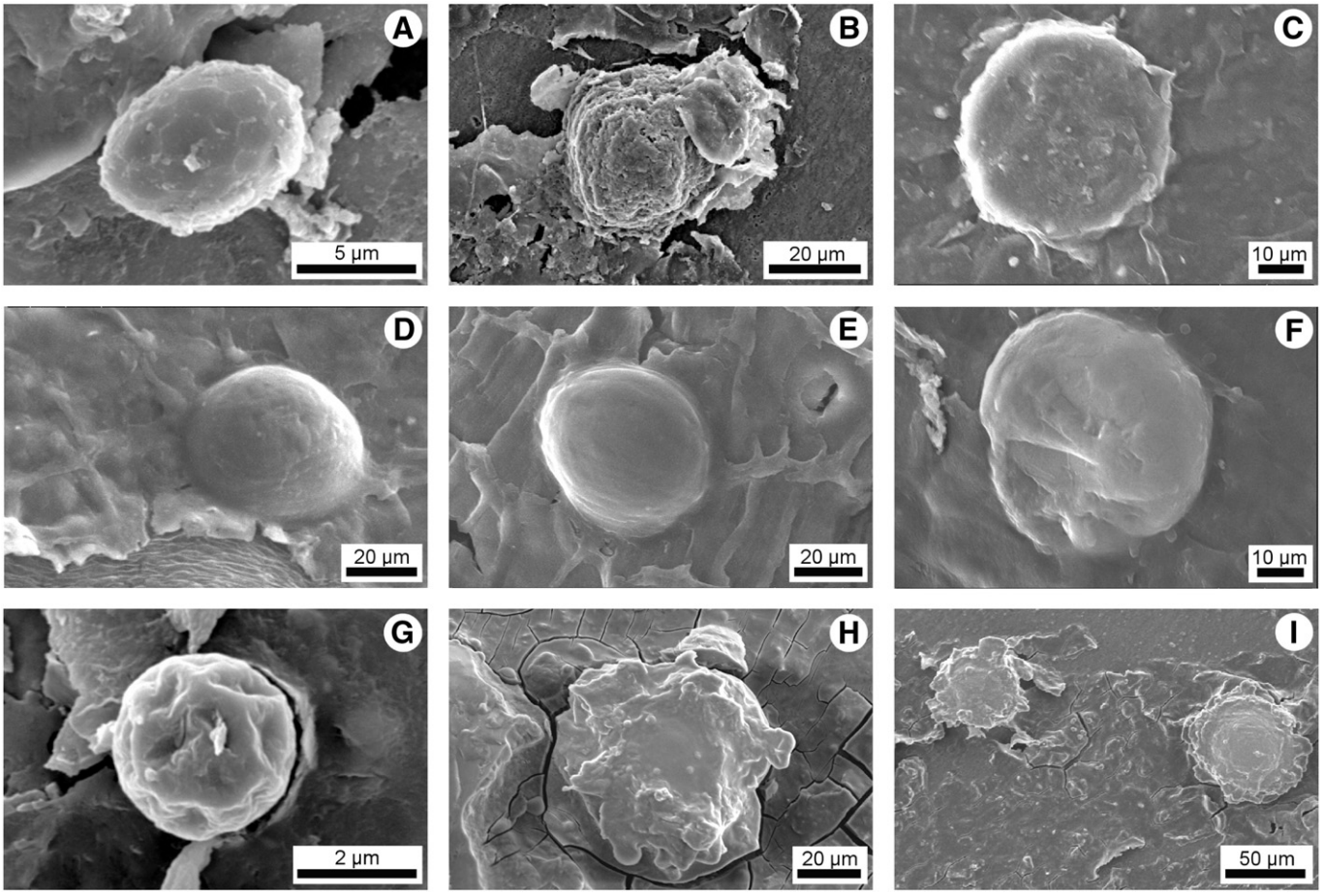

Fig. 8. SEM of secretory products in situ for *N. ovata* (A) to (F); and *L. rarinervis*: (G) to (I). (A) A smaller secretory product on a pinnule with outlined developing droplets (cf. Fig. 6G and H). (B) A layered secretory product. (C) A fairly intact secretory product from the position 'SO1' (Fig. 3A) for micro-FTIR. Note the circular arrangement of perforations about the periphery. (D) An intact secretory product from the upper penultimate rachis in Fig. 3A. (E) A most intact secretory product from the middle part of the antepenultimate rachis in Fig. 3A. (F) Folded surface of a secretory product from the petiole, noting the circular arrangement of perforations peripherally. (G) Folded and contorted secretory-product surface from the 'SO2' position (Fig. 3B). (H) Fragmentary secretory product also from 'SO2'. (I) Two close-situated secretory products from 'SO4' (compare with dense distribution in Fig. 5D).

exceeded 9 μm which is outside the range of the AFM capability. This is visually confirmed by the 'uneven, rough' surfaces seen on the SEM images. However, instead AFM provided first-time samples of the cuticular topographies of *N. ovata* and *L. rarinervis* (Fig. 9A and B, respectively), and comparative nano-height profiles (Fig. 9C). It shows the absence of relief differences between the two samples, or that the profiles are similar. Noted is that the *L. rarinervis* cuticle is richer in small agglomerations or crusts, 1.5–2.5 μm diameter. In both cases, this kind of morphology can be associated with epicuticular waxes. In fact, crusts are characteristic structures composed of cuticular waxes in extant angiospermous species (compare Barthlott et al., 1998, Fig.3). Parenthetically, these authors considered the waxes of '…great systematic significance…', after studying >13,000 species over many years. Fossil waxes in medullosaleans, as a further contributory potential to lipoid chemotaxonomy, will be considered in a future contribution.

4.2.2. TEM

A select series of transmission images of secretory products from *N. ovata* and *L. rarinervis* is presented in Fig. 10A to F, and G to I, respectively, where the sample locations are marked 'TEM' and 'SO2' on Fig. 3A and B, respectively. To note is (1) the scale change from micro- to nanometers with increasing magnification, and (2) the heterogeneity of probable chemical origin that is expressed by the shades-of-gray in these high-resolution images, however subtle in appearance.

N. ovata secretory products were sectioned across to possibly include the upper and lower cuticles, and magnified in the range from 2 k to 100 k direct magnification. At the lowest magnification (2 k, Fig. 10A) nearly the entire section is shown, *alas* without the cuticle. And centrally, a darker band (marked 'CB') with accompanying folds (undulating thin, black lines) is clearly identified (enlarged to 20 k in Fig. 10D). The 'CB' probably extended to the thinned edge of the secretory product that is identified by the thinner ('TC') and the thicker ('ThC') cuticles, lower and upper, respectively, in Fig. 10C. The cuticle (Fig. 10B: arrowed) appears incoherent which is confirmed by AFM (Fig. 9A), and probably represents the abaxial surface. The lower inside part of a secretory product, i.e., at the thin cuticle, is documented in Fig. 10E which has no knife marks (no concentric lines), whereas the upper-inside part with the thick cuticle is shown in Fig. 10F.

L. rarinervis secretory products were sectioned parallel to the upper and lower cuticle as shown in Fig. 10G to I, and magnified 3 k to 10 k, respectively. In comparison with *N. ovata*, these show a multitude of gentle folds that appear randomly oriented, except maybe in Fig. 10G. Structural details are absent in either secretory product.

4.3. Micro-FTIR

In Table 2 acronyms are introduced for the nine samples of secretory products ('SP….') and the four samples of surrounding cuticles ('*Cut*….'). This is necessary in support of the conclusions reached as individual samples are discussed and shown in Figs. 14 and 15. The calculated semi-quantitative chemical ratios for each of the eleven chemical variables are the PCA input for the chemometric and kerogen analyses (see later).

IR spectra for *N. ovata* and *L. rarinervis* shown in Figs. 11 and 12 are divided into seven spectral zones for consistent interpretation. These are defined as follows:

(1) C–H aliphatic stretching (−CH_3 and –CH_2–; 2990–2700 cm^{-1}) bands, present in all of the samples analyzed, being particularly intense in the *Cut* samples.

(2) S–H and N=C=O stretching (2600–2250 cm^{-1}) in alkyl mercaptans and isocyanates. SP-*Cut* of *N. ovata* show medium to high intensity bands in this range, while they are barely detectable in the *Cut* samples of *L. rarinervis*.

(3) C≡C, C≡N, and C=C=C stretching (2260–1900 cm^{-1}) in disubstituted alkynes, nitriles, polyynes, thiocyanates, and allenes, which are recorded mainly in the SP-*Cut* samples of *N. ovata*.

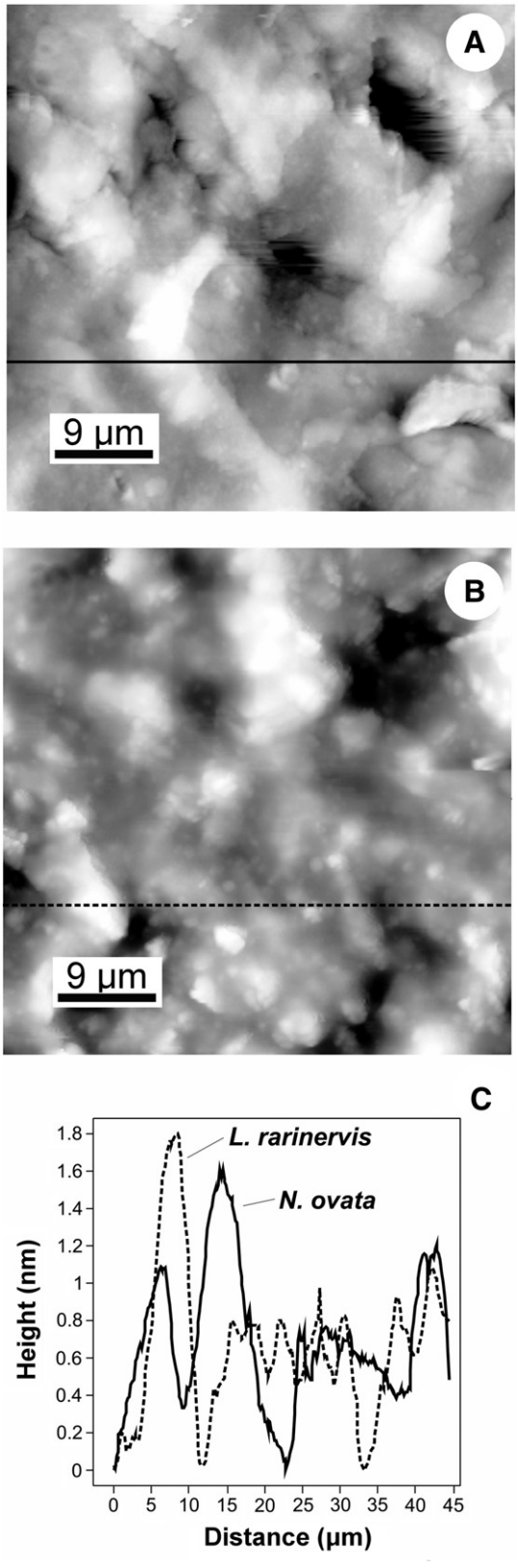

Fig. 9. AFM surfaces of the cuticular samples *N. ovata* and *L. rarinervis*. Waxy crusts (A) *N. ovata*. (B) *L. rarinervis*. (C) Height profiles (see text).

(4) C=O and C=C aromatic ring stretching (1870–1500 cm^{-1}) in carbonyl structures (carboxylic acids, ketones and esters) and aromatic compounds are present in all of the samples, though they are particularly intense in the *Cut* samples of both taxa.

(5) $-CH_3$ and $-CH_2$ deformations (1460–1375 cm^{-1}) in aliphatic compounds. As expected in medullosalean remains (e.g., Zodrow and Mastalerz, 2007), peaks at this range are particularly intense in the *Cut* samples (see (1) above).

(6) C–O and C–O–C stretching (1279–1030 cm^{-1}) in aliphatic and aromatic ethers. These bands are relatively more intense in the *Cut* samples of both taxa.

(7) C=H and aromatic C–H out-of-plane deformations and CH_2 rocking (1000–720 cm^{-1}) in methylene chains, vinyl compounds, alkenes, and aromatic hydrocarbons. Peaks (at approximately 870, 820 and 750 cm^{-1}) assigned to aromatic C–H out-of-plane deformations are more frequent and intense in the SP samples of *L. rarinervis* than those recorded for *N. ovata*. Peaks (at approximately 850, 790 and 720 cm^{-1}) representing CH_2 rocking vibrations are present in some SP-*Cut* samples of both taxa.

Based on the above information, both SP-*Cut* samples of *N. ovata* are characterized by aromatic-compound networks having aliphatic and carbonyl structures (carboxylic acids, ketones and esters), as well as variable contents of functional groups representing likely alkyl mercaptans, isocyanates, disubstituted alkynes, nitriles, polyynes, thiocyanates, and allenes.

On the other hand, the *L. rarinervis* samples show considerable differences between SP and *Cut*. Aromatic nuclei having likely carbonyl (ester) bridges and small contents of both aliphatic side chains and (less frequent) groups such isocyanates, alkynes, nitriles, polyynes, and thiocyanates characterize SP. In turn, the *Cut* samples have a predominantly aliphatic structure with a few attached functional groups, including aromatic ether and carbonyl groups.

4.4. EDS

The surface of a secretory product and cuticle immediately surrounding it (see Fig. 8D) are represented by the EDS map in the inset, and the relative elemental amounts by the plot the intensity counts vs. energy (Fig. 13). As expected, the leading element is carbon, followed by oxygen, sulfur, nitrogen, and calcium, noting that the chlorine content is likely derived from the oxidative Schulze's potassium-chlorate treatment. Hydrogen was not part of the analytical protocol. Particularly the carbon-nitrogen-oxygen-sulfur components support our interpretation of compounds based on the micro-FTIR analysis.

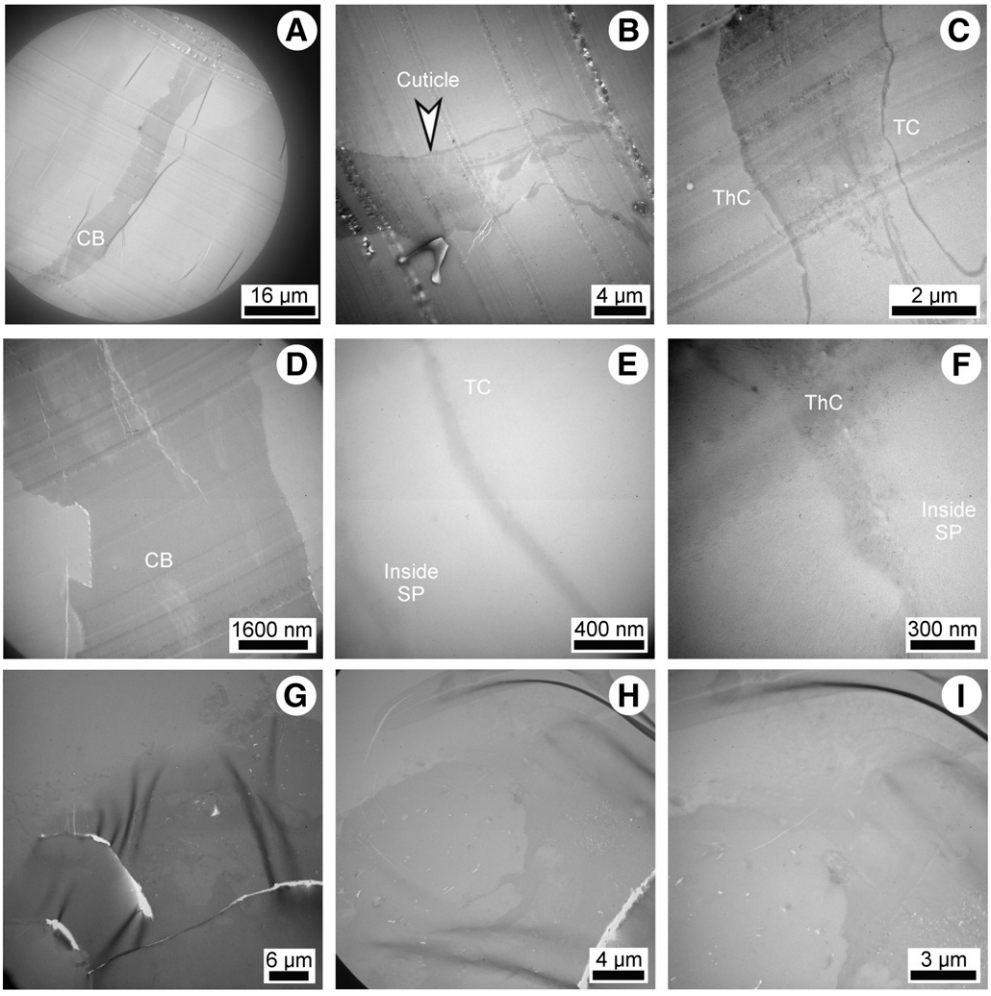

Fig. 10. TEM of secretory products in situ. *N. ovata* (A) to (F), sections: upper cuticle–secretory product–lower cuticle, and *L. rarinervis* (G) to (I), sections: parallel to upper and lower cuticles. (A) Most of a secretory product, where dark lines are folds. 'CB' = center band. The cuticle is not visible. Note: concentric light/darker bands are knife marks. (B) The cuticle. (C) At an edge, where 'TC' = thin lower cuticle, and 'ThC' = thick upper cuticle. (D) Center band 'CB' (see (A)). (E) Lower part with the thin cuticle 'TC'. No knife marks. (F) Upper part with the thick cuticle 'ThC'. (G) to (I) Prominent folds.

5. Discussion

5.1. Physical aspects

Secretory organs are regarded as evolutionary features of plants colonizing land in the Silurian-Devonian time slice, and Edwards et al. (1998, p. 261, Fig. 4 M and N) mentioned secretory functions of certain cells in Rhynie-Chert plants of the same age.

We tracked occurrences of secretory-organs from the Langsettian in the Czech Republic to the Miocene in Germany. In the Carboniferous Sydney Sub-Basin, they occurred practically throughout the entire 2100 m thick section, prominently in *Cordaites* Unger, and in the long-ranging *M. scheuchzeri*, providing the distribution template of secretory organs for the Maritimes Carboniferous Basin. It is worthwhile emphasizing that the presently available experimental data could not support the presence of secretory organs in the closest living descendents of seed ferns, specifically certain cycadalean groups (see also Popa, 2000).

Admittedly, the Supplementary material, Table 1 shows paucity in respect to the ferny, lepidodendrid, sphenophyllalean, sphenopteroid, and glossopteroid group representations, amongst others. However, for the sphenophyllalean group Batenburg (1981, Pl. VI, 9) described '…..hexangular … rounded cells (40–70 μm in diameter…..)' which Schönfeld and Storch (1979), and Storch (1980) considered to be secretory mesophyllous cells (compare with Fig. 7E). A secretory product is unmistakably imaged by Barthel (1997, Pl. I, 4) in a cuticle of *Sph. cuneifolium* (Sternberg). For sphenopteroid representation, Barthel (1962, p. 41) mentioned 'subepidermale Drüsen' in *Sphenopteris formosa* and *S. rutaefolia*, and conjectured that such structures surely must be expected in coal and associated lithologies. As for glossopteroids, Degani-Schmidt and Guerra-Sommer (2016, Pl. 5, Fig. 1, and Pl. 9, Fig. 5) documented these secretory products from a Permian coal basin in Brazil. In the light of the above observations, it seems reasonable to assume large biomass accumulations of mainly aliphatic composition, in addition to the usual plant litter, contributing to kerogen during geological time.

The most detailed distribution of secretory organs as a result of the present study is known from the *N. ovata* frond to propose an empirical distribution pattern as follows:

ovule < **trunk** < **antepenultimate rachis** < **penultimate rachis** < **ultimate rachis** < **pinnule**,

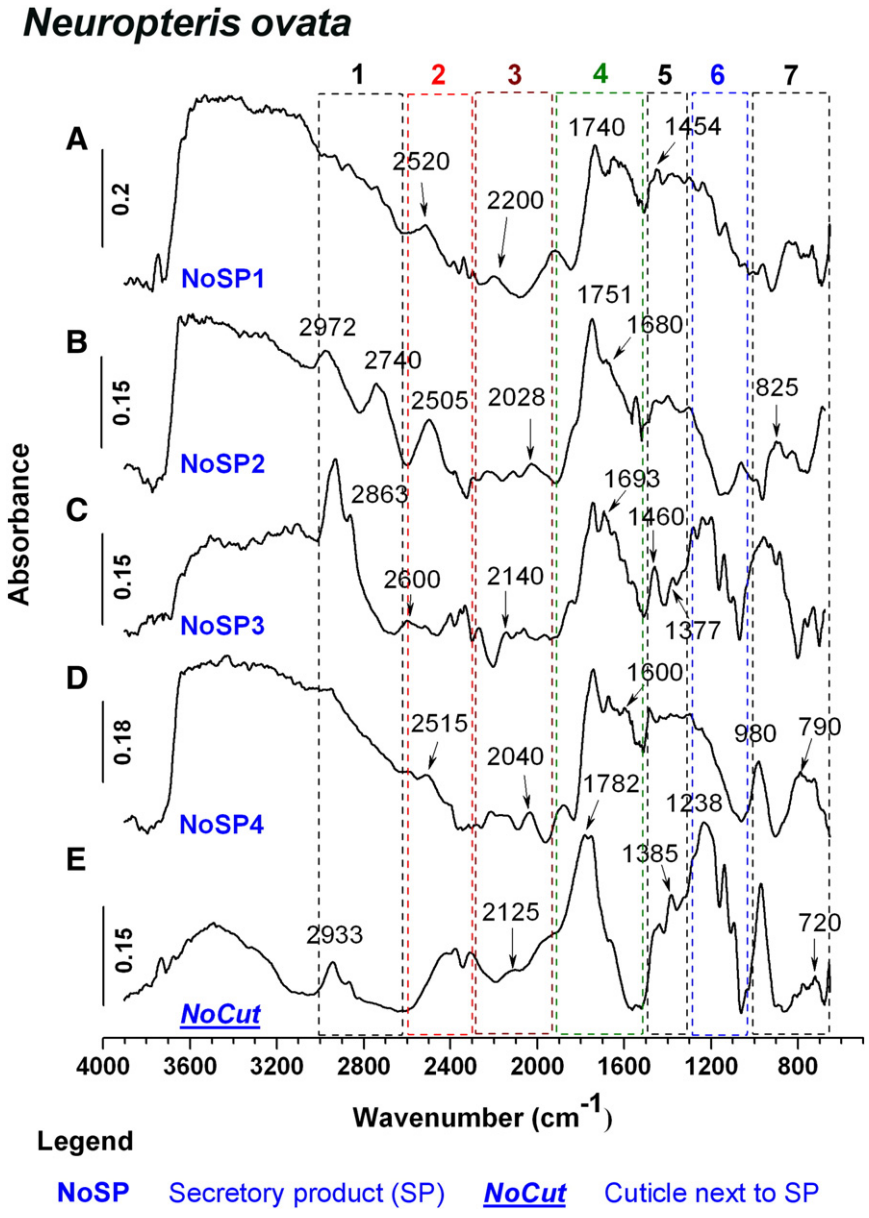

Fig. 11. Micro-FTIR spectra of *N. ovata* and their zonal divisions (see text).

where none is observed on the short pinnule midveins, and rarity exists in the integument of trigonocarpalean ovules.

To guard against misidentifying secretory organs in principle, the combination of overmacerating compressions to remove all traces of coalified mesophyllous material and ascertaining that 'dots' actually occurred inside the cuticle are prerequisites. The identification problem that arises, however, is with the larger medullosalean frond specimens. These are expected to have abundant secretory organs, but instead show abundant structural holes within appropriate diametric ranges with 'dentate collars', but rare occurrences of secretory products themselves. A prime example is the 45-cm *Alethopteris ambigua* pars (Lesquereux) frond Zodrow and Cleal, 1998 from which only three secretory products were identified in 120 slides (two are shown in Fig. 5G).

However, a 'dentate collar' by itself is not conclusive evidence for a secretory organ. Rather, it is a manifestation of fossilized intercellular, or cellular matter that coalesced (between anticlinal walls) preserving thereby on the cuticle a 'dentate collar' with a darker hue. A modern example of the schizogenesis/lysigenesis process is demonstrated by the extant leaf stomata in *C. rumphii*.

Moreover, reported are also round trichomatous bases with or without papillate 'dentate collars' (e.g., Šimůnek, 1999, Text-Fig. 1D), in addition to the elongate-ovate trichomatous bases usually depicted in the literature, dating back at least to Gothan (1916). A discussion, however, regarding the structures of trichomatous bases and association with papillae is beyond the scope of this paper.

What emerged from the present study, supported by experimental evidence (Zodrow and D'Angelo, 2016 MS), is that structural holes per se are inconclusive evidence for passageways (ducts) of secretory products. However, SEM identified instances where they are clearly encircled by regular-spaced small ca. 1 μm perforations whose function is presently unresolved. In the absence of any other known discriminating features, the presence of these perforations offers the best chances yet for identifying secretory organs, in the absence of secretory products. Further work involving microanalytical methods that combine TEM with focused ion-beam microscopy (FIB) would be beneficial for clarification (cf. Benedetti et al., 2016).

Indubitably confirmed by SEM are the observations by NICI that secretory products without exception were fossilized as spheroidal bodies, as would be expected of droplets with lipoid composition. Noted is that those (*N. ovata*) with intact surfaces lacked evidence for shrinkage, or showed a layering effect that appears parallel, or nearly so, to the cuticular surfaces. This is supported by TEM microscopy. SEM also demonstrated a diversity of 'damaged' spheroids, thereby exposing layered internal structure that likely correlate with the heterogeneous chemistry (see TEM).

Frond position and intact secretory products co-vary in *N.ovata,* in the sense that the thicker rachial cuticles (including petiolar cuticles) probably provided relatively more protection from damaging situations than the thin pinnule cuticles.

On balance, AFM could not clarify local height characteristics on the surfaces of secretory products, but provided new insights into the irregular microtopography of the cuticles which we interpreted as waxy crust with implications for both chemotaxonomy and genesis of kerogen.

5.2. Qualitative micro-IR information

IR peaks frequently found in fossilized cuticles, compressions, cuticles, and related sedimentary organic materials (e.g., coals) are also found amongst the data of Table 2. More significantly, detected were also peaks that are exclusively present in our IR data. These are assigned to stretching vibrations of single, double and triple chemical bonds involving carbon, oxygen, nitrogen, and sulfur (see confirmatory EDS). They include C–H stretching modes of CH_3 attached to O or N (Zone 1: 2850–2700 cm^{-1}, Figs. 11 and 12); S=H stretching in alkyl mercaptans (?) (Zone 2: region 2600–2540 cm^{-1}); and N=C=O, C≡C, C≡N, C=C=C stretching modes in isocyanates, disubstituted alkynes, nitriles, polyynes, thiocyanates, and allenes. Those compounds are presumably derived from the diagenetic alteration of resin-like compounds e.g., terpenoid- or phenolic-related structures (e.g., Lyons et al., 1982; van Bergen et al., 1995). This information is in agreement with our previous results (D'Angelo and Zodrow, 2016), where pinnule samples of *N. ovata* have relatively higher values of C=C cont, CH_{ar}/CH_{al}, and $CH_{ar}/C{=}C$ ratios than rachial structures. The latter could be related to possible polycyclic-aromatic hydrocarbons derived from terpenoid resins (see Table 3 of D'Angelo and Zodrow, 2016) contained in resin ducts.

Though our IR-derived information remains to be confirmed, it seems reasonable to consider that possibly naturally occurring polyynes and related chemical species are preserved. Known is a wide range of extant plants that synthesize polyynes (i.e., "polyacetylenes"), which

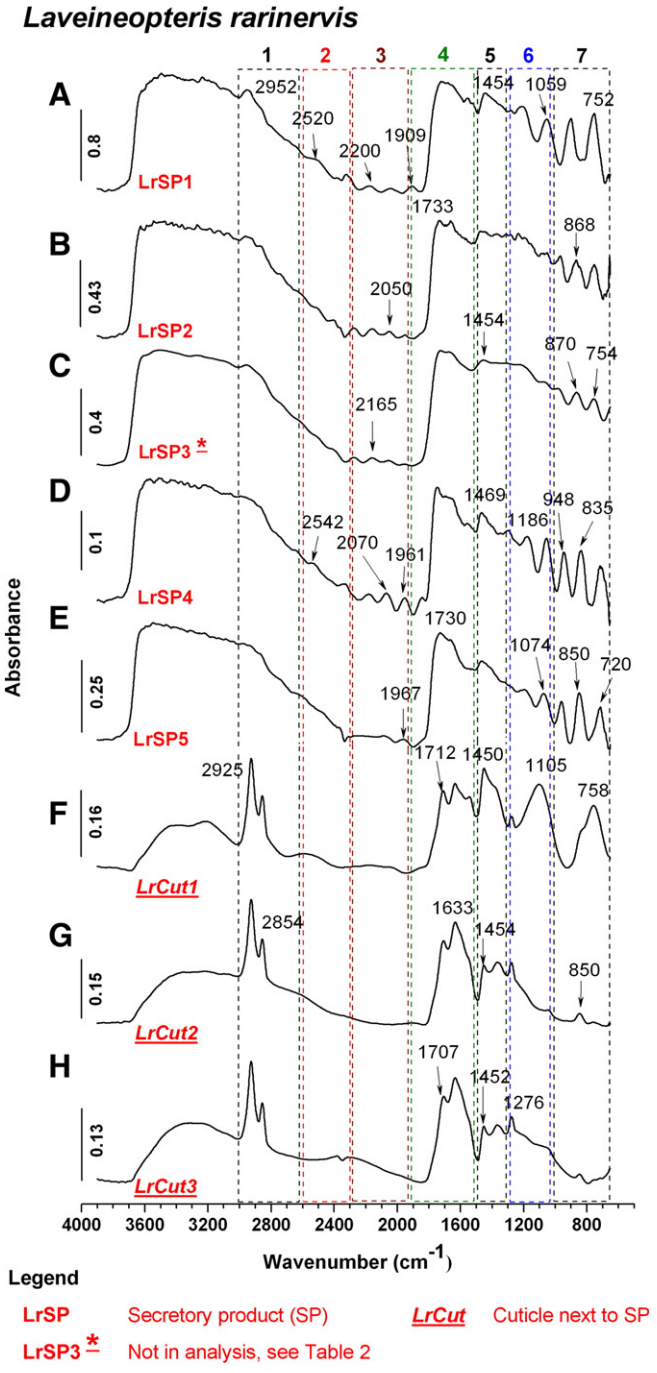

Fig. 12. Micro-FTIR spectra of *L. rarinervis* and their zonal divisions (see text).

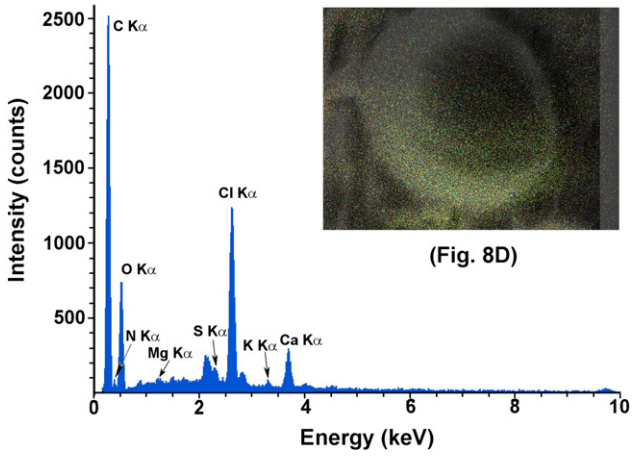

Fig. 13. EDS map of the secretory product of *N. ovata* (inset Fig. 8D), and relative elemental concentrations thereof.

play different biological roles, including flavorings and pigments and toxins as chemical repellants (e.g., Annabelle et al., 2006; Minto and Blacklock, 2008). Under certain conditions some polyynes can be fairly stable, even under unfavorable conditions of moisture and oxygen (Lagow et al., 1995). The presence of trace amounts of protein-related compounds is not impossible, provided adequate preservation conditions prevailed. Extreme examples of the preservation of labile molecules are the spectroscopic detection of amino acids (e.g., glycine) in many primitive meteorites (e.g., Altwegg et al., 2016 and references therein), as well as a number of organic molecules in interstellar dust (e.g., Papoular, 2001).

5.3. Lipoid chemotaxonomy: quo vadis?

The distinguished phytochemist R. Hegnauer (1986, p. 1524) was probably the first to recognize the potential, and to advocate the use, of secondary metabolites from extant higher plants for chemotaxonomic purposes. At the same time, he laid out important *caveats* relating to local chemical polymorphism (by mutation or hybridization), where phytochemistry would provide much further understanding. These ideas are in part integrated with the palaeochemotaxonomy proposals particularly for the seed ferns of which this study is an initial attempt in regards to lipoid taxonomy, but nevertheless forms a special aspect of our original concept of chemotaxonomy as espoused by Lyons et al. (1995). This expands the scope of our latest contribution on the chemical taxonomy of Pennsylvanian seed ferns (D'Angelo and Zodrow, 2015).

The plot of the PCA loadings is shown in Fig. 14A. Admittedly, the sample population is not large enough to derive fiducial results, nevertheless Fig. 14B presents our initial chemometric model (PC scores: see also D'Angelo et al., 2010, 2011; D'Angelo and Zodrow, 2016). This model is of considerable interest for two reasons *in potentia:*

(1) The NoSP and LrSP samples are completely separated into two distinct chemical groups, with implications for chemotaxonomic utility. The differences between the two sample groups are mainly attributed to the higher contribution of aromatic structures (C=C cont) present the *N. ovata* (especially NoSP1 and NoSP4), and the higher contents of aliphatic- and carbonyl-bearing compounds recorded for *L. rarinervis* (particularly LrSP4 and LrSP5 samples).

(2) Whereas the *NoCut* and NoSP samples show considerable functional-group overlap, LrSP and *LrCut* do not as they clearly form two separate chemical groups. *LrCut's* are characterized and distinguished from LrSP's by the lowest contents of C=O structures (see C=O/C=C values) as well as the relatively highest values recorded for the CHal/C=O ratio.

Whereas the statistical separation of NoSP and LrSP is an unexpected, but encouraging experimental result, expected were the *Cut* chemical signatures as surrogate for the schizo-lysi-rhexigenous origins, where LrSP-*LrCut* separation implies rhexigenesis, and the NoSP-*NoCut* overlap schizo-lysigenesis (see Fig. 6).

5.4. Comparison with coal macerals and kerogen types

In Fig. 15 our semi-quantitative IR data (Table 2) are compared with some available IR data from coal macerals having similar rank, Ro max 0.52%–1.41% (Mastalerz and Bustin, 1996; Guo and Bustin, 1998). Particularly depicted is a plot of 'A' vs. 'C' factors which is similar to the traditional van Krevelen H/C – O/C plot used to evaluate similarities with

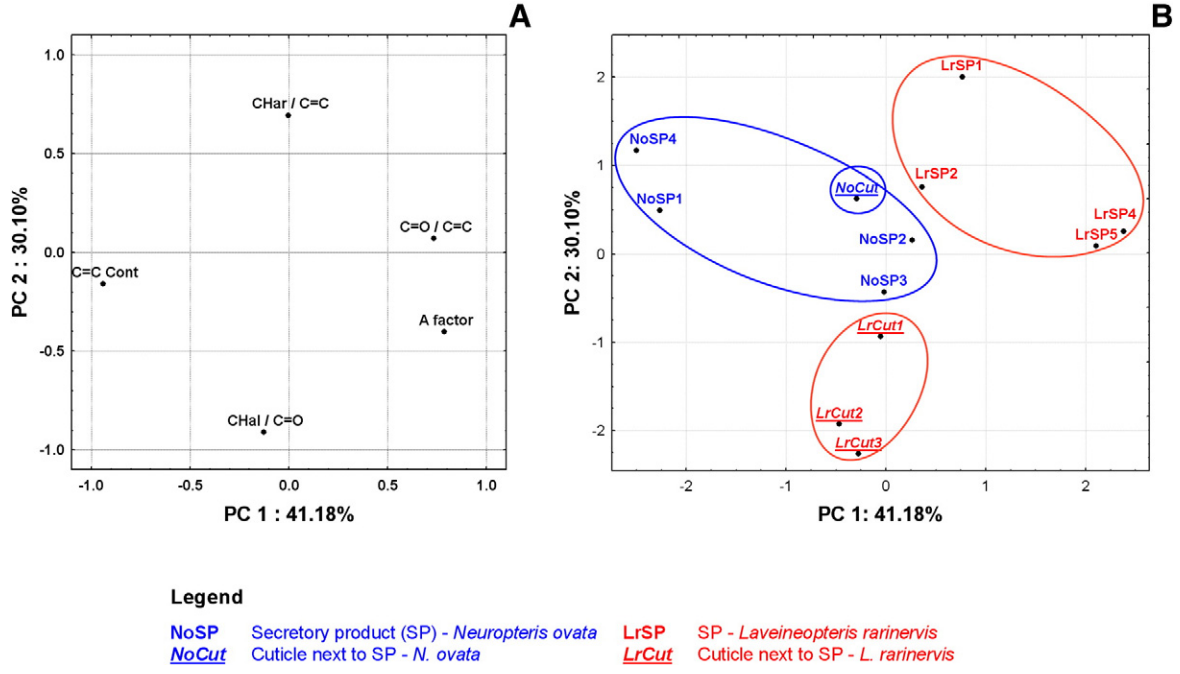

Fig. 14. Principal component analysis. (A) Plot of component loadings. (B) Plot of scores of the two-principal component model (71.28% explained variance) (see text).

different types of kerogen (see definition in Ganz and Kalkreuth, 1987). Changes in the relative intensities of the aliphatic groups are represented by the 'A' factor, while the 'C' factor represents changes in the carbonyl groups (further details can be found in Supplementary material, Table 2). Fig. 15B is a simplified plot of Fig. 15A, indicating the approximate regions for the NoSP-*NoCut* and LrSP-*LrCut* samples (ellipses around the groups do not have any statistical significance).

The SP's of both taxa plot as Type II kerogen, showing high values of 'A' and 'C' factors, which is interpreted as being a relatively high contribution by aliphatic and oxygen-containing compounds, respectively. The only exception is NoSP4, which is Type III Kerogen as indicated by its 'A' factor value i.e., the lowest of the complete data set (Table 2). NoSP4 can be regarded as the most chemically altered specimen.

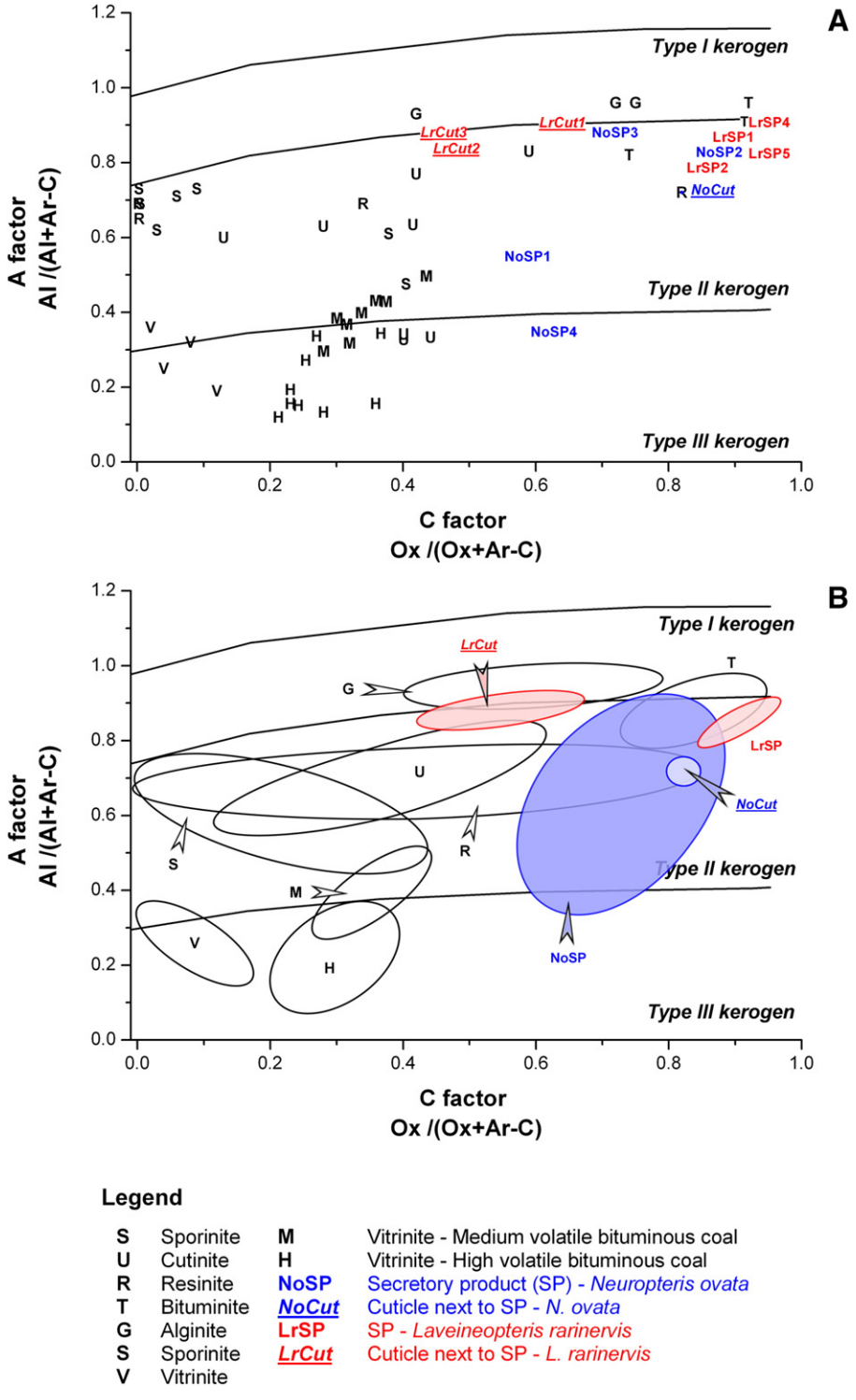

Fig. 15. Kerogen-type diagram of micro-FTIR data compared to some coal macerals. (A) Simplified plot of traditional van Krevelen H/C vs. O/C plot. (B) Simplified plot of (A) showing approximate regions of the sample forms.
Sources of coal macerals (IR data): Mastalerz and Bustin (1996; cutinite, vitrinite of medium and high volatile bituminous coals), and Guo and Bustin (1998; cutinite, resinite, bituminite, alginite and vitrinite).

LrSP1, LrSP2, LrSP4, and LrSP5 have 'A' and 'C' factor values which are very similar to those exhibited by NoSP2 and *NoCut*, denoting a similar chemistry.

LrSP1, LrSP2, LrSP4, and LrSP5 are similar in composition to some bituminites while NoSP1 to NoSP4 (and *NoCut*) show a functional-group chemistry similar to some bituminites and cutinites (Fig. 15). *LrCut1* to *3* are better described by their chemical similarities with some alginites and cutinites (Fig. 15).

The micro-FTIR data and coal macerals (mainly alginites, bituminites, and cutinites) shared a similar thermal history, as inferred from similarities in some of their functional groups such as similar distributions and similar relative contents (e.g., 'A' factor and 'C' factor). Inferred from this is that secretory organs (including cuticles) contributed to the origin of kerogen.

5.5. Proposed definition of a lipoid fossil-secretory organ

The definition of a fossil secretory organ as a secondary metabolite producer includes two concepts. One is an inhomogeneous-layered, aliphatic exudate theoretically composed of compounds such as isocyanates, disubstituted alkynes, nitriles, polyynes, thiocyanates and allenes presumably derived from the resin-like compounds, terpenoid- or phenolic-related chemical structures. Polyynes perform a variety of biological functions (e.g., toxins, repellent). This is collectively named eigenchemistry (nov. nomenclature) to differentiate it from the chemistry of the plant-fossil cutin itself, and also from the schizo-, lysigenously influenced cuticle near a secretory product. The second concept relates to the duct structure of which we have only preliminary information: it is circular, apparently smooth, and shows a ring of evenly spaced, very small structural holes about its periphery in the cuticle; compare with Bode (1929, Fig. 1).

6. Conclusion

This study introduces into palaeobotany the concept of secretory organs as a potentially valuable microchemical parameter with implication for kerogen genesis. The secretory product (exudate) is of variable lipoid composition which is inferred from the heterogenic internal structure exposed by damaged secretory organs, but remains to be confirmed by micro-FTIR of oriented TEM sections.

What mirrors our approach to attaining a natural classification system, as opposed to Brongniart's model of morphology, is that the chemotaxonomic potential rests not only with the exudates themselves, but more generally with combining parameters of morphology with its microchemistry. This includes the chemistry of coalified compressions as taxonomic-chemical-characters. We caution that the presence/absence itself of secretory organs in medullosaleans (or ferns) alone cannot be considered a taxonomic parameter (morphological character), reiterating Bode's insights.

Additionally, secretory organs could be of environmental/ecological significance e.g., an adaptation to environmental stress or a defense mechanism against pathogens.

Based on some commonly shared chemical characteristics found in Kerogen Types II/III, some coal macerals (i.e., cutinite, alginite, and bituminite) and our data, we postulate that the functional groups characterizing secretory products and surrounding cuticles are related to the propensity to generate kerogen and the subsequent oil and gas/condensate. The evidence suggests that secretory organs are abundant and widespread particularly in fossil foliage (and that products are regenerative) which implies a considerable contribution of resin-like materials to the overall chemistry of foliar remains. Hence, with *caveats* we suggest that secretory products contributed significantly to amorphous kerogen accumulations in the sedimentary column. Future research is recommended in

(1) IR and EDS mapping based on intact sectioned secretory organs to fine-tune the understanding of internal chemical heterogeneity, and compound identification;

(2) Questions of whether or not fossil-exudate chemistry can confirm/deny conspecificity, heeding Hegnauer's *caveats*?

(3) Clarifying the structural characteristics of exudate passages; and

(4) Establishing efficient criteria for secretory-organ recognition in the absence of secretory products.

Acknowledgements

Reviewers of the MS (anonymous and Dr. C. Eble) are cordially thanked for thoughtful, complimentary, and encouraging suggestions and remarks regarding presentation and focusing of arguments. Remarks by the editor are equally appreciated, and heeded.

We thank Ms. L. DiGironimo and Dr. D. Stevenson (The New York Botanical Garden) for the leafy material of *C. rumphii*, collected by the former (accession number 581/2006-F) from the Nolen Greenhouse, 2014, and for the ovules collected by the latter from the Montgomery Botanical Center, Coral Gables, FL.; particularly, the accession number for *C. rumphii* is 981804-G. Dr. Z. Šimůnek (Czech Geological Survey, Prague) donated the 40 cordaitean slides for which we are more than grateful. A monetary contribution from Cape Breton University (to Curator E.L. Zodrow) for the SEM and EDS analyses, performed by Mr. Stephen Kelloway of the Verschuren Centre (Cape Breton University), is gratefully acknowledged.

Appendix A. Supplementary data

Supplementary data to this article can be found online at http://dx.doi.org/10.1016/j.coal.2016.10.004.

References

Adinew, B., 2014. GC–MS and FT-IR analysis of constituents of essential oil from *Cinnamon* bark growing in South-west Ethiopia. I. J. Herbal Med. 1 (6), 22–31.
Altwegg, K., Balsiger, H., Bar-Nun, A., Berthelier, J.-J., Bieler, A., Bochsler, P., et al., 2016. Prebiotic chemicals-amino acid and phosphorus-in the coma of comet 67P/Churyumov-Gerasimenko. Sci. Adv. 2 (e1600285), 1–5.
Annabelle, L.K., Shun, S., Tykwinski, R.,.R., 2006. Synthesis of naturally occurring polyynes. Angew. Chem. Int. Ed. 45, 1034–1057.
Barrier, S., 2008. Physical and Chemical Properties of Sporopollenin Exine Particles PhD Thesis Univ. Hull, UK (273 pp., plus appendices).
Barthel, M., 1961. Der Epidermisaufbau einiger oberkarbonischen Pteridospermen. Geologie 7, 828–849.
Barthel, M., 1962. Epidermisuntersuchungen an einigen inkohlten Pteridospermen blättern des Oberkarbons und Perms. Geol. Beih. 33, 1–140.
Barthel, M., 1997. Epidermal structures of sphenophylls. Rev. Palaeobot. Palynol. 95, 115–127.
Barthlott, W., Neinhuis, C., Cutler, D., Ditsch, F., Meusel, I., Theissen, I., Wilhelm, H., 1998. Classification and terminology of plant epicuticular waxes. Bot. J. Linn. Soc. 126, 237–260.
Bashforth, A.R., 2005. Late Carboniferous (Bolsovian) macroflora from the Barachois Group, Bay St. George Basin, southern Newfoundland, Canada. Palaeontogr. Can. 24, 1–123 (20 pls).
Batenburg, L.H., 1981. Vegetative anatomy and ecology of *Sphenophyllum zwickaviense*, *S. emarginatum*, and other "Compression species" of *Sphenophyllum*. Rev. Palaeobot. Palynol. 32, 275–313.
Benedetti, A., Diez, J.B., Sender, L.M., Escapa, I., Cúneo, R., 2016. New application of FIB: a 3D look into the past throughout the ultrastructure of fossil plant cuticles. Microsc. Microanal. 22 (Suppl. S4), 8–9.
Bertrand, P., 1930. Bassin houiller de la Sarre et de la Lorraine. I. Flore fossile. 1. Neuroptéridées. Étude Gîtes Minereaux de France. 1–58 (Text-figs. 1–8, pls. 1–30).
Bode, H., 1929. Sekretionsorgane bei *Mariopteris latifolia* Brgt. Jahrb. Preuss. Geol. Landesan., Berlin, Bd. XLIX, Teil II. pp. 795–800.
Braune, W., Leman, A., Taubert, H., 1999. Pflanzenanatomisches Praktikum I. Zur Einführung in die Anatomie der Samenpflanzen. Spektrum Akademischer Verlag, Heidelberg (368 pp.).
Bunbury, C.J.F., 1847. On fossil plants from the coal formation of Cape Breton. J. Geol. Soc. Lond. 3, 423–438 (pls. 4).
Calder, J.H., 1998. The Carboniferous evolution of Nova Scotia. In: Blundell, D.J., Scott, A.C. (Eds.), Lyell: the Past is the Key to the Present. Geol. Soc., London, Spec. Public. 143, pp. 261–302.
Chadwick, D.J., Whelan, J. (Eds.), 1992. Secondary Metabolites: Their Function and Evolution. Ciba Foundation Symposium 171. John Wiley & Sons, New York, p. 318.

Chen, Y., Zou, C., Mastalerz, M., Suyun, H., Gasaway, C., Toa, X., 2015. Applications of micro-Fourier Transform Infrared spectroscopy (FTIR) in the geological sciences—a review. Int. J. Mol. Sci. 15, 30223–302550. http://dx.doi.org/10.3390/ijms161226227.
Cleal, C.J., Shute, C.H., 2012. The systematic and palaeoecological value of foliage anatomy in Late Palaeozoic medullosalean seed-plants. J. Syst. Palaeontol. 10, 765–800.
Cleal, C.J., Shute, C.H., Zodrow, E.L., 1990. A revised taxonomy for Palaeozoic neuropterid foliage. Taxon 39, 486–492.
Cleal, C.J., Zodrow, E.L., Mastalerz, M., 2010. An association of *Alethopteris* foliage, *Trigonocarpus* ovules and *Bernaultia*-like pollen organs from the Middle Pennsylvanian of Nova Scotia, Canada. Palaeontogr. B 283, 73–97.
Colthup, N.B., Daly, L.H., Wiberley, S.E., 1990. Introduction to Infrared and Raman Spectroscopy. Academic Press, New York, p. 547.
D'Angelo, J.A., 2006. Analysis by Fourier transform infrared spectroscopy of Johnstonia (Corystospermales, Corystospermaceae) cuticles and compressions from the Triassic of Cacheuta, Mendoza, Argentina. Ameghiniana 43 (4), 669–685.
D'Angelo, J.A., Zodrow, E.L., 2015. Chemometric study of structural groups in medullosalean foliage (Carboniferous, fossil Lagerstätte, Canada): Chemotaxonomic implications. Int. J. Coal Geol. 138, 42–54.
D'Angelo, J.A., Zodrow, E.L., 2016. 3D chemical map and a theoretical life model for *Neuropteris ovata* var. *simonii* (index fossil, Asturian, Late Pennsylvanian, Canada). Int. J. Coal Geol. 153, 12–27.
D'Angelo, J.A., Zodrow, E.L., Camargo, A., 2010. Chemometric study of functional groups in Pennsylvanian gymnosperm plant organs (Sydney Coalfield, Canada): Implications for chemotaxonomy and assessment of kerogen formation. Org. Geochem. 41, 1312–1325.
D'Angelo, J.A., Escudero, L.B., Volkheimer, W., Zodrow, E.L., 2011. Chemometric analysis of functional groups in fossil remains of the *Dicroidium* flora (Cacheuta, Mendoza, Argentina). Int. J. Coal Geol. 87, 97–111.
Degani-Schmidt, I., Guerra-Sommer, M., 2016. Epidermal morphology and ecological significance of *Glossopteris pubescens* nom. nov. from the Brazilian Permian (Samarian). Rev. Palaeobot. Palynol. 232, 119–139.
DiMichele, W.A., Rischbieter, M.O., Eggert, D.L., Gastaldo, R.A., 1984. Stem and leaf cuticles of *Karinopteris*: source of cuticles from the Indiana 'paper' coal. Am. J. Bot. 71, 626–637.
Edwards, D., Kerp, H., Hass, H., 1998. Stomata in early land plants: an anatomical and ecophysiological approach. J. Exp. Bot. 49, 255–278.
Ellis, E.A., 2006. Corrected formulation for Spurr low viscosity embedding medium using the replacement epoxide ERL 4221. Microsc. Microanal. 12, 288–289.
Fahn, A., 1979. Secretory Tissues in Plants. Academic Press, New York, p. 302.
Forgeron, S., MacKenzie, B., MacPherson, K., 1986. The effects of geological features on coal mining, Sydney coalfield, Nova Scotia. CIM Bull. 79, 79–87.
Ganz, H., Kalkreuth, W., 1987. Application of infrared spectroscopy to the classification of kerogen-types and the evolution of source rock and oil–shale potentials. Fuel 66, 708–711.
Gothan, W., 1916. Über die Epidermen einiger Neuropteriden des Carbons. Jahrb. König. Preuss. Geol. Landesan., Berlin, Band XXXV, Teil II. pp. 373–381 (1914).
Guo, Y., Bustin, R.M., 1998. Micro-FTIR spectroscopy of liptinite macerals in coal. Int. J. Coal Geol. 36, 259–275.
Hacquebard, P.A., 1984. Coal rank changes in the Sydney and Pictou Coalfields of Nova Scotia; cause and economic significance. CIM Bull. 77, 33–40.
Hegnauer, R., 1986. Phytochemistry and plant taxonomy—an essay on the chemotaxonomy of higher plants. Phytochem. 25, 1519–1535.
Heredia-Guerrero, J.A., Benitez, J.J., Dominguez, E., Bayer, I.S., Cingolani, R., Athanassiou, A., Heredia, A., 2014. Infrared and Raman spectroscopic features of plant cuticles: a review. Plant. Sci. 5, 1–14 (Article 305).
Hoffmann, F., 1827. Über die Pflanzenreste des Kohlenbebirges von Ibbenbühren und vom Piesberge bei Osnabrück. In: Keferstein, C. (Ed.), Teutschland geognostisch-geologisch dargestellt. 4, pp. 150–160 (Weimar, Figuren 1–10).
Kauppinen, J.K., Moffatt, D.J., Mantsch, H.H., Cameron, D.G., 1981a. Fourier transform in the computation of self-deconvoluted and first order derivative spectra of overlapped band contours. Anal. Chem. 53, 1454–1457.
Kauppinen, J.K., Moffatt, D.J., Mantsch, H.H., Cameron, D.G., 1981b. Fourier self-deconvolution: a method for resolved intrinsically overlapped bands. Appl. Spectrosc. 35, 271–276.
Kögel-Knabner, I., De Leeuw, J.W., Tegelaar, E.W., Hatcher, P.G., Kerp, H., 1994. A lignin-like polymer in the cuticle of spruce needles: implications for the humification of spruce litter. Org. Geochem. 21, 1219–1228.
Krings, M., 2000. Remains of secretory cavities in pinnules of Stephanian pteridosperms from Blanzy-Montceau (Central France): a comparative study. Bot. J. Linn. Soc. 132, 369–383.
Lagow, R.J., Kampa, J.J., Wei, H.C., Battle, S.L., Genge, J.W., Laude, D.A., Harper, C.J., Bau, R., Stevens, R.C., Haw, J.F., Munson, E., 1995. Synthesis of linear acetylenic carbon: The "sp" carbon allotrope. Science 267 (5196), 362–367.
Leisman, G.A., 1960. The morphology and anatomy of *Callipteridium sullivanti*. Am. J. Bot. 47, 281–287.
Lin, R., Ritz, G.P., 1993a. Reflectance FT-IR microspectroscopy of fossil algae contained in organic-rich shale. Appl. Spectrosc. 47, 265–271.
Lin, R., Ritz, G.P., 1993b. Studying individual macerals using i.r. microspectroscopy, and implications on oil versus gas/condensate proneness and "low-rank" generation. Org. Geochem. 20, 695–706.
Litke, R., 1966. Kutikularanalytische Untersuchungen im Niederlausitzer Unterflöz. Paläobot. Abhand. B, Bd. II. pp. 328–426 (Heft 2, pls. XXXIX).
Lyons, P.C., Finkelman, R.B., Thompson, C.L., Brown, F.W., Hatcher, P.G., 1982. Properties, origin and nomenclature of rodlets of the inertinite maceral group in coals of the central Appalachian Basin, U.S.A. Int. J. Coal Geol. 1, 313–346.
Lyons, P.C., Orem, W.H., Mastalerz, M., Zodrow, E.L., Vieth-Redemann, A., Bustin, R.M., 1995. 13 C NMR, micro-FTIR and fluorescence spectra, and pyrolysis-gas chromatograms of coalified foliage of late Carboniferous medullosan seed ferns, Nova Scotia. Canada: implications for coalification and chemotaxonomy. Int. J. Coal Geol. 27, 227–248.
Lyons, P.C., Zodrow, E.L., Millay, M.A., Dolby, G., Gillis, K.S., Cross, A.T., 1997. Coal-ball floras of Maritime Canada and palynology of the Foord seam: geologic, palaeobotanical and paleoecological implications. Rev. Palaeobot. Palynol. 95, 31–50.
Mastalerz, M., Bustin, R.M., 1993a. Electron microprobe and micro-FTIR analyses applied to maceral chemistry. Int. J. Coal Geol. 24, 333–345.
Mastalerz, M., Bustin, R.M., 1993b. Variation in maceral chemistry within and between coals of various ranks: and electron microprobe and micro-FTIR investigation. J. Microsc. 171, 153–166.
Mastalerz, M., Bustin, R.M., 1996. Application of reflectance micro-Fourier Transform infrared analysis to the study of coal macerals: an example from the Late Jurassic to Early Cretaceous coals of the Mist Mountain Formation, British Columbia, Canada. Int. J. Coal Geol. 32, 55–67.
Minto, R.E., Blacklock, B.J., 2008. Biosynthesis and function of polyacetylenes and allied natural products. Prog. Lipid Res. 47, 233–306.
Papoular, R., 2001. The use of kerogen data in understanding the properties and evolution of interstellar carbonaceous dust. Astron. Astrophys. 378, 597–607.
Petersen, H.I., Nytoft, H.P., 2006. Oil generation capacity of coals as a function of coal age and aliphatic structure. Org. Geochem. 37, 558–583.
Petersen, H.I., Rosenberg, P., Nytoft, H.P., 2008. Oxygen groups in coals and alginite-rich kerogen revisited. Int. J. Coal Geol. 74, 93–113.
Popa, M., 2000. Aspects of Romanian Early Jurassic palaeobotany and palynology. Part II. A new species of *Pachypteris* from Cristian. Rev. Palaeobot. Palynol. 111, 31–47.
Pryor, J.S., 1990. Delimiting species among permineralized medullosan pteridosperms: a plant bearing *Alethopteris* frond from the Upper Pennsylvanian of the Appalachian basin. Can. J. Bot. 68, 184–192.
Rochdi, A., Landais, P., 1991. Transmission micro-infrared spectroscopy: an efficient tool for microsample characterization of coal. Fuel 70, 367–371.
Roliff, W.A., 1962. The Maritimes Carboniferous basin of eastern Canada. Proc. Geol. Assoc. Can. 14, 21–41.
Schönfeld, C., Storch, D., 1979. Einsatz des Auflichtmikroskops Vertical in der paläobotanischen Arbeit. Jenaer Rundschau 24 (6), 242–245.
Šimůnek, Z., 1996. Leaves and cuticles of the genus *Lesleya* Lesquereux from the Czech Republic and from Illinois (U.S.A.). In: Leary, R.L. (Ed.), Patterns in Palaeobotany. Proceeding of a Czech–U.S. Carboniferous Palaeobotany Workshop, Illinois State Mus. Sci. Papers 26, pp. 43–56.
Šimůnek, Z., 1999. Cuticles of *Neurodontopteris auriculata* (Brongniart) Potonié from the Stephanian B of the Czech Republic. Acta Univ. Carol. Geol. 43, 625–631.
Smith, B.C., 1996. Fundamentals of Fourier Transform Infrared Spectroscopy. CRC Press, London, p. 202.
Sobkowiak, M., Painter, P., 1992. Determination of the aliphatic and aromatic CH contents of coals by FT-i.r.: studies of coal extracts. Fuel 71, 1105–1125.
Storch, D., 1980. *Sphenophyllum*-Arten aus drei intramontanen Karbonbecken: Pflanzengeographische Besonderheiten im mittel europäischen Karbon. Schriftenr. Geol. Wissen. 16, 171–273 Berlin.
Tsubaki, S., Azuma, J., 2013. Total fractionation of green tea residue by microwave-assisted alkinepretreatment and enzymatic hydrolysis. Bios. Technol. 131, 485–491.
van Bergen, P.F., Collinson, M.E., Scott, A.C., de Leeuw, J.W., 1995. Unusual resin chemistry from Upper Carboniferous pteridosperm resin rodlets. In: Anderson, K.B., Crelling, J.C. (Eds.), Amber, Resinite and Fossil ResinsSymposium Series 617. Am. Chem. Soc, Washington, D.C., pp. 149–169.
Wang, Z.-Q., 1997. Permian *Supaia* fronds and an associated *Autunia* fructificationfrom Shanxi, China. Palaeont. 40, 245–277.
Wang, S.H., Griffiths, P.R., 1985. Resolution enhancement of diffuse reflectance i.r. spectra of coals by Fourier self-deconvolution. 1. C-H stretching and bending modes. Fuel 64, 229–236.
Zodrow, E.L., Cleal, C.J., 1988. The structure of the Carboniferous pteridosperm frond *Neuropteris ovata* Hoffmann. Palaeontogr. B 208, 105–124.
Zodrow, E.L., Cleal, C.J., 1998. Revision of the pteridosperm foliage of *Alethopteris and Lonchopteridium* (Upper Carboniferous), Sydney Coalfield, Nova Scotia, Canada. Palaeontogr. B 247, 65–122.
Zodrow, E.L., D'Angelo, J.A., 2014. *Cycas rumphii* as a Model for the Larger Carboniferous Medullosalean Ovule. 4th Internat. Palaeon. Congr., Abst Mendoza, Argentina p. 839.
Zodrow, E.L., D'Angelo, J.A., 2016. *Alethopteris ambigua* (Lesquereux 1884) Pars: New Microanalytical Insights (Compression, Seed-fern Attributes, Canada). MS.
Zodrow, E.L., Mastalerz, M., 2007. Functional groups in a single pteridosperm species: variability and circumscription (Pennsylvanian, Nova Scotia, Canada). Int. J. Coal Geol. 70, 313–324.
Zodrow, E.L., Mastalerz, M., 2009. A proposed origin for fossilized Pennsylvanian plant cuticles by pyrite oxidation (Sydney Coalfield, Nova Scotia, Canada). Bull. Geosci. 84, 227–240.
Zodrow, E.L., Vasey, G.M., 1986. Mabou Mines section: biostratigraphy and correlation (Pennsylvanian Pictou Group, Nova Scotia, Canada). J. Paleontol. 60, 208–232.
Zodrow, E.L., Šimůnek, Z., Bashforth, A.R., 2000. New cuticular morphotypes of *Cordaites principalis* from the Canadian Carboniferous Maritimes Basin. Can. J. Bot. 78, 135–148.
Zodrow, E.L., Helleur, R., Werner-Zwanziger, U., Banghao, C., D'Angelo, J.A., 2013. Spectrochemical study of coalified *Trigonocarpus grandis* (Pennsylvanian tree-fern ovule, Canada). Int. J. Coal Geol. 109–110, 24–35.
Zodrow, E.L., D'Angelo, J.A., Al-Shra'ah, A., 2014. Morphology and histochemistry of coalified *Trigonocarpus grandis* (Sydney Coalfield, Canada): implications for the preservation, chemotaxonomy, and evolution of Carboniferous medullosalean ovules. Int. J. Coal Geol. 122, 61–75.